THE UNIVERSITY OF MICHIGAN
COLLEGE OF LITERATURE, SCIENCE, AND THE ARTS
Department of Physics

Technical Report No. 18

A STUDY OF THE REACTION $p+p \rightarrow d+\pi^+$ FROM 1 TO 2.8 BEV

Richard M. Heinz

ORA Project 03106

under contract with:

DEPARTMENT OF THE NAVY
OFFICE OF NAVAL RESEARCH
CONTRACT NO. Nonr-1224(23)
WASHINGTON, D.C.

administered through:

OFFICE OF RESEARCH ADMINISTRATION ANN ARBOR

October 1964

This report was also a dissertation submitted in partial fulfillment of the requirements for the degree of Doctor of Philosophy in The University of Michigan, 1964.

A STUDY OF THE REACTION $p+p \rightarrow d+\pi^+$ FROM 1 TO 2.8 BEV

By Richard Meade Heinz

ABSTRACT

The purpose of this investigation was to perform an experimental and theoretical study of the reaction $p+p \rightarrow d+\pi^+$ in the BeV region. The differential and total cross sections for this reaction have been measured with scintillation counters for incident proton kinetic energies of 1.0, 1.3, 1.5, 1.7, 2.0, 2.5, and 2.8 BeV, using the external proton beam of the Cosmotron of Brookhaven National Laboratory. Values of the differential cross section are given for barycentric deuteron angles, θ, for $0 \geq \cos\theta \geq -.97$ in small intervals of $\cos\theta$. From 1.3 to 2.0 BeV, as $\cos\theta$ varies from -0.5 to -1.0, the differential cross section rises, passes through a pronounced maximum, and then decreases rapidly. This maximum propagates from $\cos\theta = -0.8$ at 1.3 BeV to $\cos\theta = -.94$ at 2.0 BeV and evolves into a sharp peak at $\cos\theta = -1.0$ for energies above 2.0 BeV. The total cross section decreases rapidly and monotonically with energy from 450 μb at 1.0 BeV to 30 μb at 2.8 BeV.

A theoretical calculation is made using the one-nucleon exchange peripheral model, and the data are compared with this and with the one-pion exchange model and the statistical model. The only theoretical success is obtained with the one-nucleon exchange model, which qualitatively explains the

observed angular distributions of the differential cross section above 1.0 BeV in terms of the strong repulsive core which exists in the nucleon-nucleon central interaction potential; it also shows that the rapid decrease of the total cross section with energy is expected because of the structure of the deuteron momentum space wave function.

ACKNOWLEDGEMENTS

I am very grateful to Dr. Oliver Overseth for his invaluable contributions to the experiment and for his guidance during the past two years; his outstanding qualities as a physicist and advisor have made it a very rewarding and gratifying experience to have had him as my doctoral committee chairman.

Dr. Martin Perl deserves many thanks for the important part which he played in the experiment. I would also like to thank Dr. Lawrence Jones, Dr. Michael Longo, David Pellett, Fred Martin, Homer Neal, Howard Saxer, and the staff of the Cosmotron for their help in the experiment.

I am extremely thankful to Dr. Marc Ross for the extensive help he gave me in the theoretical parts of this thesis, and I also appreciate discussions with Dr. Perl and Dr. Jones concerning the one-nucleon exchange model.

Finally, I would like to thank the National Science Foundation for the financial support it has given me while in graduate school.

TABLE OF CONTENTS

LIST OF TABLES

LIST OF FIGURES

I. INTRODUCTION

A. THE REACTION $p + p \rightarrow d + \pi^+$

The primary interest in studying the reaction $p + p \rightarrow d + \pi^+$ is that it is one of the few two body reactions in high energy particle physics, and therefore might provide both a stimulus and a test for dynamical theories of particle interactions. Perl *et al.*[1] have pointed out that the simplest Feynman diagram for this reaction is the one-nucleon exchange, shown in Fig. 1; this diagram is calculated in the next chapter. Yao[2] and Chahoud *et al.*[3] have studied this reaction in terms of a one-pion exchange model, corresponding to the Feynman diagrams in Fig. 2. Using the statistical model[4], a prediction is made by R. Hagedorn[5] of the energy dependence of the differential cross section at 90°. These theories are discussed in the next chapter.

A further interest in the reaction stems from the results of Turkot *et al.*[6] and Cocconi *et al.*[7] who measured a single point in the differential cross section near 0° at various energies. Their combined results when plotted versus energy[7] show a peak in the forward differential cross section at 2.5 BeV incident kinetic energy.

B. SURVEY OF EXISTING DATA

At energies below 1 BeV, investigations by others[8] find the differential cross section for this reaction rises to a broad maximum at $\cos\theta = 1.0$ (θ is the barycentric deuteron

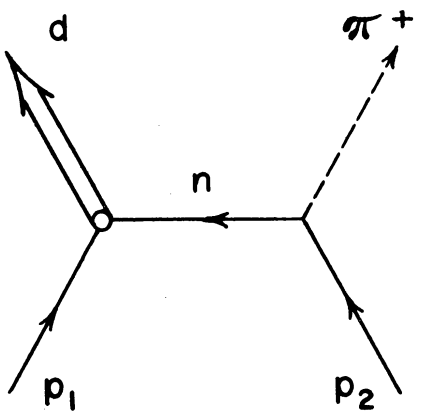

Fig. 1. One-nucleon exchange Feynman diagram for the reaction $p+p \rightarrow d+\pi^+$.

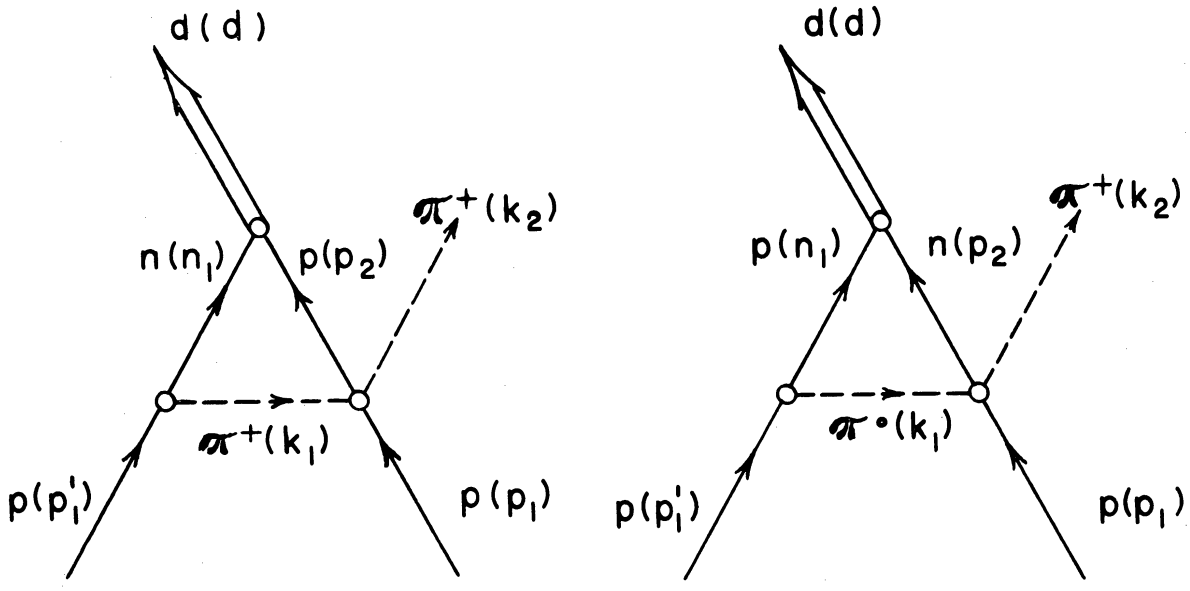

Fig. 2. One-pion exchange Feynman diagrams for the reaction $p+p \rightarrow d+\pi^+$.

angle) over a considerable range of energies. Homer et al.[9], measuring the deuteron momentum spectrum at 8.2° in the laboratory for .991 BeV protons, give evidence of a dip occurring in the forward c.m. direction. Although the results of Bugg et al.[10] at 97 BeV are consistent with the dip, the angular distribution from this bubble chamber data is not well established because of the small number of events (42); similarly, the cloud chamber experiment of Batson et al.[11] at .97 BeV yielded only 4 events. However, very recent data from Chapman et al.[12] at .99 BeV give the angular distribution from $\cos\theta = 0$ to $\cos\theta = .9$ and the cross section does appear to be reaching a broad maximum in the forward direction.

Subsequent to this experiment, Dekkers et al.[15] published values for the differential and total cross sections for the reaction $\pi^+ + d \rightarrow p+p$, which, using the principle of detailed balance, are equivalent to the $p+p \rightarrow d+\pi^+$ cross sections at the same barycentric angle and energy. The relevant transformations are[16]

$$\frac{d\sigma}{d\Omega}(p+p \rightarrow d+\pi^+) = \frac{3}{4}\frac{q^2}{p^2}\frac{d\sigma}{d\Omega}(\pi^+ + d \rightarrow p+p)$$

and

$$\sigma_{Total}(p+p \rightarrow d+\pi^+) = \frac{3}{2}\frac{q^2}{p^2}\sigma_{Total}(\pi^+ + d \rightarrow p+p)$$

where q and p are the magnitudes of the $\pi^+ d$ and pp c.m. momenta respectively. All of the cross sections measured in our experiment except those at 1.0 BeV can be corroborated by this data.

The remaining experimental information in the energy region from 1 to 3 BeV consists of total cross section measurements by Sechi-Zorn[13] at 2.05 BeV and Smith *et al.*[14] at 2.85 BeV. All of the data mentioned above is presented graphically and compared with the results of this experiment in Chapter VI.

II. THEORY

A. ONE-NUCLEON EXCHANGE MODEL

The one-nucleon exchange model was suggested by Perl *et al.*[1] to explain the processes $\pi^- + p \rightarrow \bar{p} + d$ ($\bar{p}$ is antiproton), $p + p \rightarrow d + \pi^+$, and backward pion-nucleon elastic scattering, and has been used by Bernstein[17] and Nearing[18] as a model for intermediate boson production in the reaction $p + p \rightarrow d + W^+$. Cook *et al.*[19] have carried out the pion-nucleon calculation but find it gives a result which is too high by one or two orders of magnitude. However, this model has been useful in low energy nuclear physics in the theory of direct interactions.[20]

In the Feynman diagram for this model (Fig. 1), the two incoming protons, p_1 and p_2, have four-momenta p_1 and p_2, while d, k and n are the four-momenta of the outgoing deuteron and pion and the exchanged neutron, respectively. The masses of the particles which are on the mass shell are such that

$$p_1^2 = p_2^2 = -M^2, \quad k^2 = -\mu^2, \quad \text{and} \quad d^2 = -M_d^2.$$

The R-matrix element for this diagram can be written down directly and is given by

$$R_1 = \left(\frac{-i}{\hbar c}\right)^2 \int d^4n \, (2\pi)^4 \, \delta^4(k-n-p_2)(2\pi)^4 \, \delta^4(d-n-p_1)$$

$$\left[\frac{i}{(2\pi)^4} \frac{1}{i\not{n}+M+i\epsilon} i\sqrt{2}\, G\, \gamma_5 \left(\frac{1}{2\pi}\right)^{3/2} \sqrt{\frac{M}{p_{2_0}}}\, u(p_2)\right]^T \left(\frac{1}{2\pi}\right)^{3/2} \Gamma$$

$$\left(\frac{1}{2\pi}\right)^{3/2} \sqrt{\frac{M}{p_{1_0}}}\, u(p_1) \left(\frac{1}{2\pi}\right)^{3/2} \sqrt{\frac{1}{2k_0}}$$

where $\bar{\Gamma}=\gamma_4\Gamma^\dagger\gamma_4$, Γ is the neutron-proton-deuteron vertex function, and the superscript T indicates the transpose and arises because of the way in which the spin part of the deuteron wave function is expressed, as will be seen below. G is the pion-nucleon coupling constant, $G^2/4\pi\approx 15$. The total matrix element, R, is the difference between R_1 and R_2, where R_2 is obtained from R_1 by interchanging P_1 and P_2. The relativistically invariant matrix elements, M_1 and M_2, are defined by

$$R_1=(2\pi)^4\ \delta^4(d+k-p_1-p_2)\ M_1\left[\left(\frac{1}{2\pi}\right)^{3/2}\right]^4 N_d N_k N_p{}^2$$

and similarly for M_2, where N_a is the normalization factor for the a^{th} particle.

In terms of $M=M_1-M_2$, the cross section is

$$d\sigma=\frac{(2\pi)^{-2}\left[N_d N_k N_p{}^2\right]^2}{F}\ |M|^2\ \delta^4(d+k-p_1-p_2)p_{1_0}p_{2_0}d^3d\ d^3k$$

where $$F=(p_1\cdot p_2)^2-p_1{}^2p_2{}^2$$

is the invariant flux term. Specializing to the barycentric system,

$$\frac{d\sigma}{d\Omega}=\left(\frac{1}{2\pi}\right)^2\left(\frac{M}{U}\right)^2\frac{M_d}{2}\ \frac{p_f}{p_i}\ \frac{1}{4}\ \Sigma\,|M|^2$$

where U is the total c.m. energy, p_f and p_i are the magnitudes of the final and initial c.m. three-momenta, respectively, and Σ indicates a sum over deuteron and proton spin states. We also have

$$M_1=\sqrt{2}\ G\left[\frac{1}{i\not{p}_1+M+i\epsilon}\ \gamma_5\ u(p_2)\right]^T\bar{\Gamma}u(p_1)$$

and

$$M_2 = \sqrt{2}\, G\left[\frac{1}{i\not{n}_2 + M + i\epsilon}\,\gamma_5\, u(p_1)\right]^T \bar{\Gamma}\, u(p_2),$$

where $n_1 = p_2 - k$ and $n_2 = p_1 - k$.

Before proceeding with the evaluation of the matrix element, it is necessary to develop an expression for Γ. Blankenbecler *et al.*[21] and Goldberger *et al.*[22] have studied this vertex function and, neglecting the deuteron D-state, express it as $\Gamma = \frac{4\pi N}{M} S$, where M, the nucleon mass, should not be confused with the matrix element M; N is the normalization of the deuteron wave function, given by

$$N^2 = \frac{\alpha}{2\pi}\,\frac{1}{1-\alpha\rho}$$

where $\alpha = \sqrt{BM}$, B is the magnitude of the deuteron binding energy, and ρ is the effective range of the deuteron.[22] S is the deuteron triplet spin function. As shown in reference 21, instead of expressing it as a 16 component column vector, it can be written in terms of Dirac matrices as

$$S = \frac{M_d - i\not{d}}{2M_d}\,\frac{\gamma\cdot\epsilon}{\sqrt{2}}\, C$$

where ϵ is the deuteron polarization vector and $C = i\gamma_4\gamma_2$ is the charge conjugation matrix, $C^2 = 1$ and $C\gamma_\mu C = -\gamma_\mu^T$. However, this expression for Γ is only valid in the limit $\varkappa^2 = -\alpha^2$ where $\varkappa$ is magnitude of the three-momentum of the neutron or proton inside the deuteron. This limit is equivalent to taking both the proton and neutron as being on the mass shell. For this problem $\varkappa_1^2$ (subscript refers to M_1 or M_2) can be found by evaluating the equation $d^2 = (n_1 + p_1)^2$ in the

deuteron rest frame, and is given by

$$\varkappa_1^2 = \frac{1}{2}\left[M_d^2 - 2M^2 + (n_1^2 + M^2)\right] + p_1 \cdot d + \left(\frac{p_1 \cdot d}{M_d}\right)^2$$

(similarly for $\varkappa_2^2$). For the energy range from 1 to 2.8 BeV, $\varkappa$ ranges from 10α to 43α and clearly a general expression $\Gamma(\varkappa)$ must be found.

If the spin dependance of Γ is removed by writing $\Gamma = HS$, then H can be written in the non-relativistic limit as $H = \langle \varphi(\underline{r}) | V(\underline{r}) | e^{-i\underline{\varkappa}\cdot\underline{r}} \rangle^{23}$ where $\underline{r}$ is the relative coordinate between the neutron and proton, $\varphi(\underline{r})$ is the internal wave function of the deuteron, and $V(\underline{r})$ is the central force nuclear interaction potential (since the D-state probability for the deuteron is only $\approx 4\%$, the tensor force is neglected). The Schrödinger equation for the deuteron is

$$\left[-\frac{\nabla^2}{M} + V(\underline{r})\right]\varphi(\underline{r}) = -B\varphi(\underline{r})$$

where M is twice the reduced mass of a neutron and proton; it follows that

$$H = -\frac{1}{M}\langle \varphi(\underline{r}) | BM - \nabla^2 | e^{-i\underline{\varkappa}\cdot\underline{r}} \rangle$$

or

$$H = -\frac{1}{M}(\alpha^2 + \varkappa^2)\langle \varphi(\underline{r}) | e^{-i\underline{\varkappa}\cdot\underline{r}} \rangle .$$

Thus H is proportional to $(\alpha^2 + \varkappa^2)$ times the momentum space deuteron wave function. The function

$$F(\varkappa) \equiv \frac{\alpha^2 + \varkappa^2}{4\pi N}\langle \varphi(\underline{r}) | e^{-i\underline{\varkappa}\cdot\underline{r}} \rangle$$

is a most important quantity in this model and will be discussed further. Note that since $\Gamma = \frac{4\pi N}{M} S\, F(\varkappa)$ (neglecting

phase), if Γ is to be consistent with the Γ given in references 21 and 22 and used by Yao in the one-pion exchange calculation[2] (see Section B), then $F(\varkappa) = 1$ when $\varkappa^2 = -\alpha^2$.

For the Hulthén phenomenological deuteron wave function given by Hulthén et al.[24] as

$$\varphi(r) = \frac{N}{r}\left[e^{-\alpha r} - e^{-\beta r}\right],$$

we find

$$F(\varkappa) = \frac{\beta^2 - \alpha^2}{\beta^2 + \varkappa^2} .$$

Because of this form of $F(\varkappa)$, it will henceforth be referred to as the deuteron vertex form factor. Blankenbecler et al.[25] have derived the same expression for $F(\varkappa)$ by using dispersion relations.

Another wave function which will be considered is a hard core wave function

$$\varphi(r) = 0, \quad r < r_c$$
$$\varphi(r) = \frac{N}{r} e^{-\alpha r}\left[1 - e^{-\beta(r - r_c)}\right], \quad r \geq r_c$$

which is taken from reference 24 and corresponds to a potential with an infinitely repulsive core ("hard" core) of radius r_c and the Hulthén potential for $r > r_c$. Adopting natural units for the deuteron of $\hbar = c = \alpha = 1$, the deuteron vertex form factor for this wave function is

$$F(\varkappa) = \frac{1 + \varkappa^2}{\varkappa} e^{-r_c}\left[\frac{\sin \varkappa r_c + \varkappa \cos \varkappa r_c}{1 + \varkappa^2} - \frac{(\beta+1)\sin \varkappa r_c + \varkappa \cos \varkappa r_c}{(\beta+1)^2 + \varkappa^2}\right]$$

These two form factors are shown in Fig. 3. The constant β is given in reference 24 and is chosen to make the corresponding wave functions consistent with empirical information

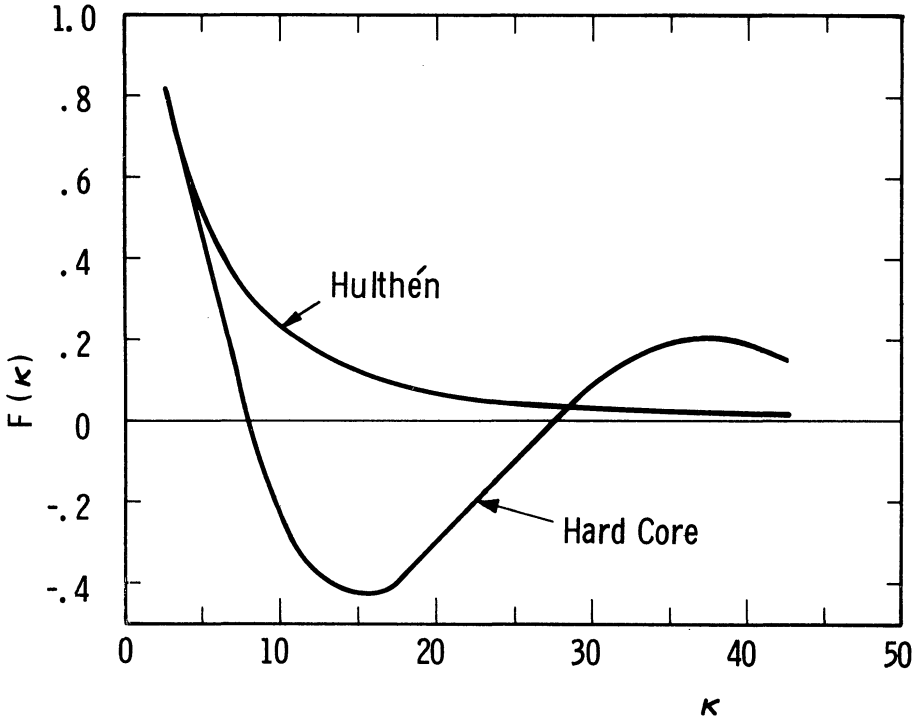

Fig. 3. The deuteron vertex form factor $F(\kappa)$ for two deuteron wave functions, the Hulthén and the hard core. κ is the magnitude of the three-momentum of either nucleon inside the deuteron. In the units used, κ=22 corresponds to a momentum of about 1 BeV/c.

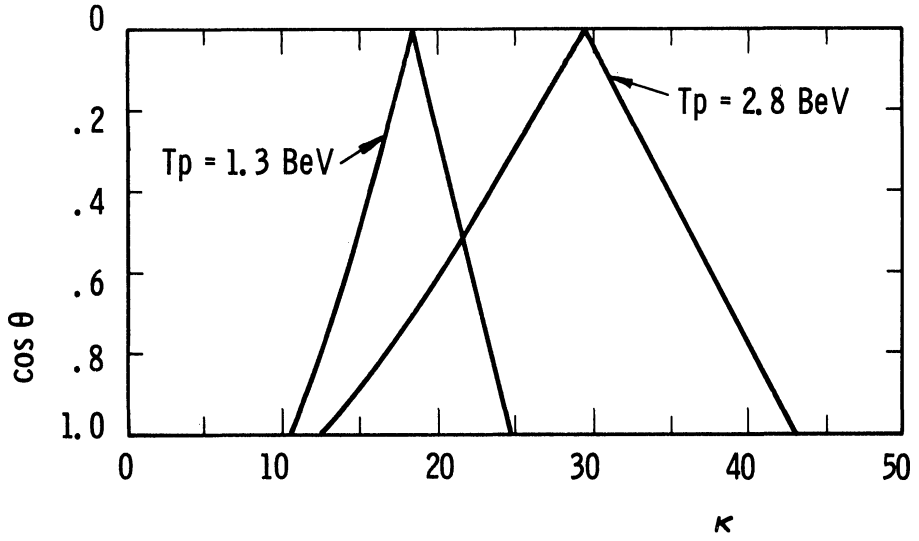

Fig. 4. The two values of κ corresponding to the cosine of the barycentric scattering angle θ for the reaction $p+p \rightarrow d+\pi^+$ in the one-nucleon exchange model. This double-valued function of θ is given for two incident proton energies, 1.3 BeV and 2.8 BeV.

on the neutron-proton system; r_c is .13 (.56F).

Salpeter et al.[26] show that several interaction potentials (Yukawa, exponential, and Gaussian) yield $F(\varkappa)$'s with shapes similar to the Hulthén potential; in addition these authors show that $F(\varkappa)$ for a repulsive core potential changes sign as does the potential itself, similar to the hard core $F(\varkappa)$ in Fig. 3. The maximum of this $F(\varkappa)$ at $\varkappa \approx 37$ is characteristic of an infinitely repulsive core and probably has no physical meaning, especially since the deuteron should be treated relativistically for $\varkappa \gtrsim 20.5$ ($\varkappa \gtrsim .938$ BeV/c).

As shown previously, for each c.m. scattering angle and energy $\varkappa$ has two values, $\varkappa_1$ and $\varkappa_2$, corresponding to the Feynman diagram in Fig. 1, and Fig. 1 with p_1 and p_2 interchanged. Fig. 4 shows this double-valued function of the scattering angle for two incident kinetic energies, 1.3 BeV and 2.8 BeV. It turns out that the diagram with the smaller value of $\varkappa$ dominates in the final cross section, so that our ignorance of $F(\varkappa)$ for $\varkappa \gtrsim 20.5$ is not too important; both diagrams are retained throughout the calculation, however.

Moreover, an examination of Figs. 3 and 4 shows that if the terms other than $F(\varkappa)$ in the calculated scattering amplitude do not vary strongly with $\varkappa$, then for the hard core deuteron wave function this model predicts (remembering that the Feynman diagram with the smaller value of $\varkappa$ dominates) that the cross section will have a maximum, and that this maximum will migrate towards 0° as the incident

kinetic energy increases, finally becoming a peak at 0°. In addition, both wave functions predict that the total cross section will decrease with energy because of the smaller probability for the occurrence of high momentum components in the momentum space deuteron wave function.

Continuing with the evaluation of $d\sigma/d\Omega$, we find (for details of the spin sums see Appendix)

$$\frac{1}{4}\Sigma |M|^2 = \frac{G^2}{M^2}\left[\frac{AF^2(n_1)}{(n_1^2+M^2)^2} + \frac{BF^2(n_2)}{(n_2^2+M^2)^2} - \frac{2CF(n_1)F(n_2)}{(n_1^2+M^2)(n_2^2+M^2)}\right]\frac{\alpha\pi}{(MM_d)^2}\frac{1}{1-\alpha\rho},$$

where

$$A = 3(MM_d - p_1\cdot d)\left[\mu^2 p_2\cdot d + 2k\cdot p_2\, k\cdot d - M\mu^2 M_d\right]$$

$$B = 3(MM_d - p_2\cdot d)\left[\mu^2 p_1\cdot d + 2k\cdot p_1\, k\cdot d - M\mu^2 M_d\right]$$

and

$$C = M^2M_d^2\mu^2 - MM_d\mu^2(p_2\cdot d + p_1\cdot d) - (k\cdot d)^2(M^2 + p_1\cdot p_2)$$
$$- MM_d\, k\cdot d(p_2\cdot k + p_1\cdot k) + \mu^2\, p_1\cdot d\, p_2\cdot d$$
$$+ p_1\cdot k\, p_2\cdot d\, k\cdot d + p_1\cdot d\, p_2\cdot k\, k\cdot d.$$

The resulting expression for the cross section is

$$d\sigma/d\Omega = \frac{G^2}{4\pi}\frac{1}{2M_dM^2U^2}\frac{\alpha}{1-\alpha\rho}\frac{p_f}{p_i}\left[\frac{AF^2(n_1)}{(n_1^2+M^2)^2} + \frac{BF^2(n_2)}{(n_2^2+M^2)^2}\right.$$
$$\left. - \frac{2CF(n_1)F(n_2)}{(n_1^2+M^2)(n_2^2+M^2)}\right].$$

An important factor must be considered before this calculation can be completed. Several authors[27-30] have pointed out that single-particle exchange models can give very misleading, if not meaningless, results unless one takes into account absorption in the initial and final state. For example, Ross *et al.*[27] have demonstrated that for the one

pion exchange model in the reaction $\pi^- + p \rightarrow \rho^0 + n$, the calculated cross section is suppressed by a factor of 1/3 in the forward direction and 1/7 in the backward direction due to this effect.

In this paper absorption will be treated in the manner developed by Ross et al.[27] The method used is similar to the distorted wave Born approximation used in low energy nuclear physics.[20] One simply makes a partial wave expansion of the scattering amplitude (M for this problem) and attenuates each partial wave by a factor $\frac{1}{2}(\eta_\ell + 1)\frac{1}{2}(\mu_\ell + 1)$ where $\eta_\ell = \exp.(-2\delta_\ell^I)$ ($\delta_\ell{}^I$ is the imaginary part of the ℓ^{th} partial wave pp phase shift) and μ_ℓ is similarly determined by the $\pi^+ d$ phase shift.

The optical theorem shows that pp diffraction scattering is almost purely imaginary, and the η_ℓ's can thus be determined by the experimental data, as given for example by Fujii et al.[31] The μ_ℓ's cannot be found in such a straightforward manner; however, if one considers $\pi^+ d$ scattering, the deuteron forms a very large target for the pion, and it is expected that although many partial waves will be affected, no phase shift will be very large and as a first approximation all the μ_ℓ's can be taken to be one. This means that the suppression factors $\frac{1}{2}(\eta_\ell + 1)\frac{1}{2}(\mu_\ell + 1)$ will generally be too large and one would expect that if the one-nucleon exchange is the dominant mechanism for the reaction $p + p \rightarrow d + \pi^+$, the calculation given in this paper will predict cross sections

somewhat higher than the experimental data. In the partial wave expansion of M, spin was neglected.

Fig. 5 shows the final cross sections for the one-nucleon exchange model at 2.0 BeV; curve A corresponds to the cross section obtained by using the hard core deuteron wave function neglecting absorption effects, while curve B represents the same wave function with absorption included. Similarly, curves C and D are calculated using the Hulthén deuteron wave function without and with the absorption suppression factors respectively. These curves show the importance of considering absorption effects.

From a detailed analysis of pp elastic scattering data, Jastrow[32] concludes that a strong repulsive singularity does exist in the nucleon-nucleon potential and uses $r_c = .6F$ to fit empirical data. Gammel et al.[33] have reached a similar conclusion, while several authors have given theoretical arguments for the existence of a repulsive core.[34] Although the evidence for such a core is not definitive, its presence is highly probable and therefore the comparison of the one-nucleon exchange model with experimental data will be made by using the hard core deuteron wave function. This comparison is shown in Figs. 6-9; the curves labeled N in these figures are the results of the one-nucleon exchange model, developed above, where a hard core of radius $r_c = .65F$ was used. The theoretical curves labeled P are from the one-pion exchange model as given by Yao[2] which will be discussed in

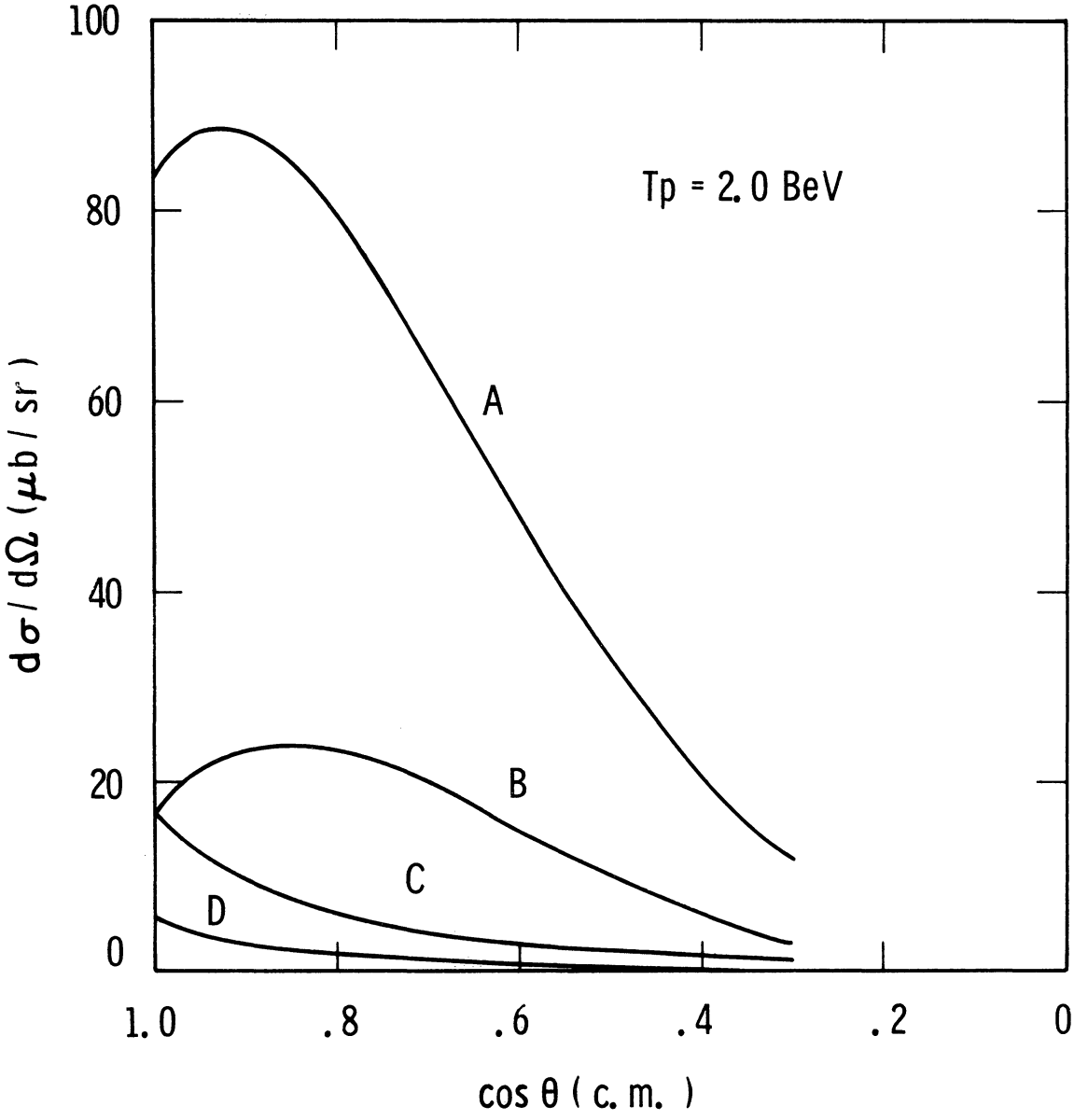

Fig. 5. Plots of one-nucleon exchange model cross sections for the reaction $p+p \rightarrow d+\pi^+$ versus the cosine of the c.m. scattering angle at 2.0 BeV incident kinetic energy. Curve A is obtained by using the hard core deuteron wave function without employing the absorption correction; B is the hard core deuteron wave function with absorption effects included; C and D correspond to the Hulthén deuteron wave function without and with the absorption suppression factors, respectively.

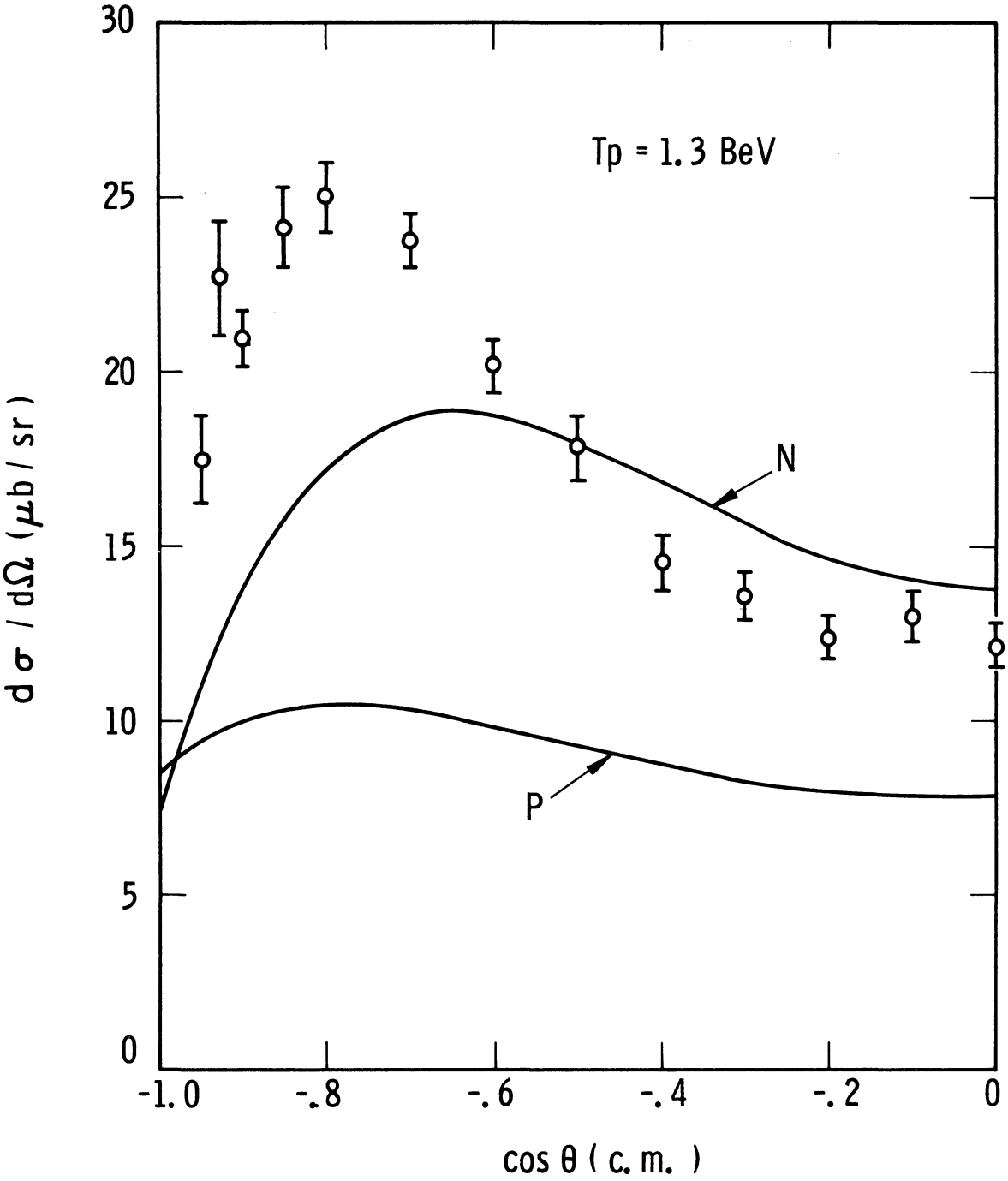

Fig. 6. One-nucleon exchange model (curve N) and one-pion exchange model (curve P) theoretical cross sections for the reaction $p+p \rightarrow d+\pi^+$ at an incident proton kinetic energy (T_p) of 1.3 BeV. The circles represent the data from this experiment.

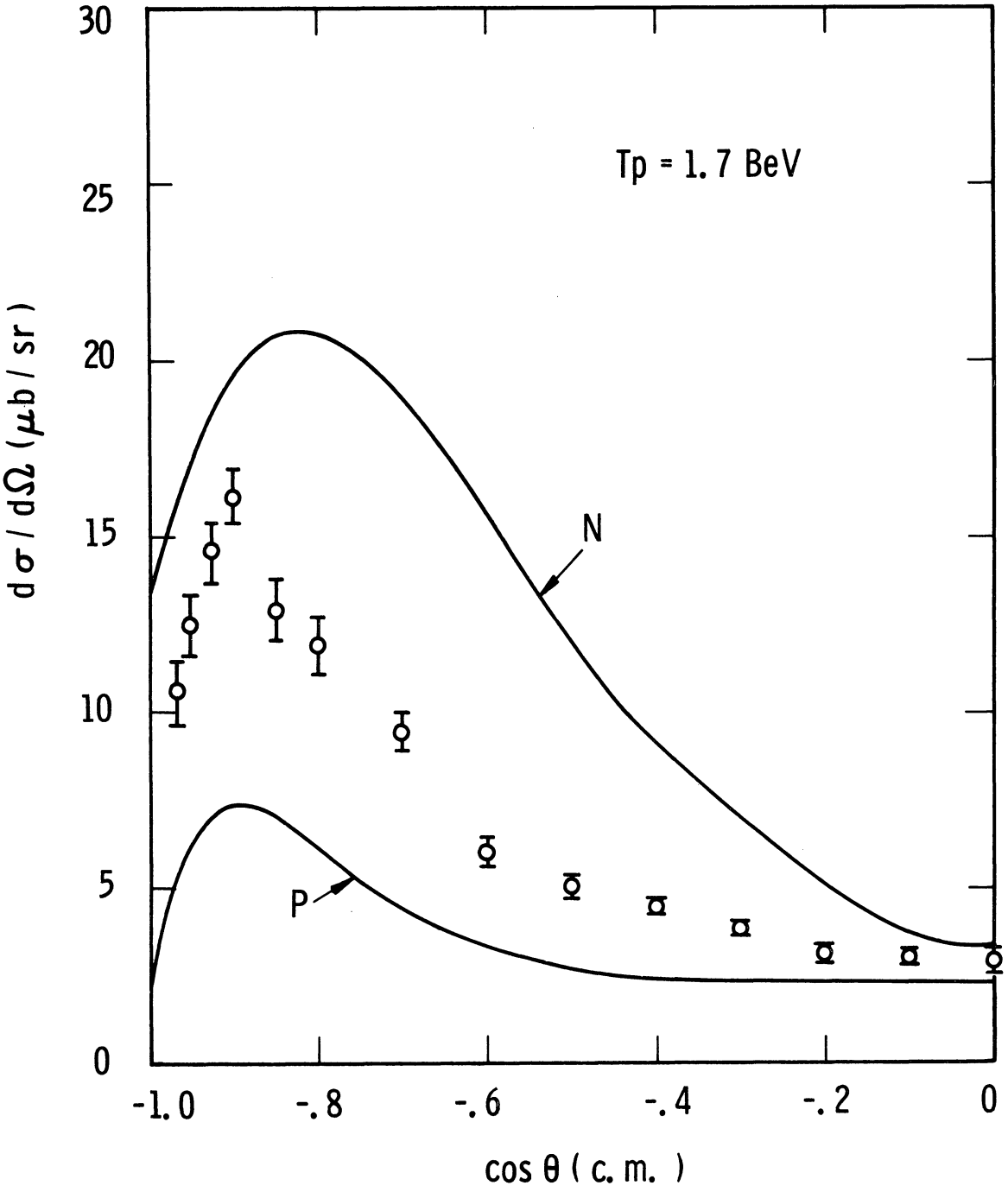

Fig. 7. One-nucleon exchange model (curve N) and one-pion exchange model (curve P) theoretical cross sections for the reaction $p+p \rightarrow d+\pi^+$ at an incident proton kinetic energy (T_p) of 1.7 BeV. The circles represent the data from this experiment.

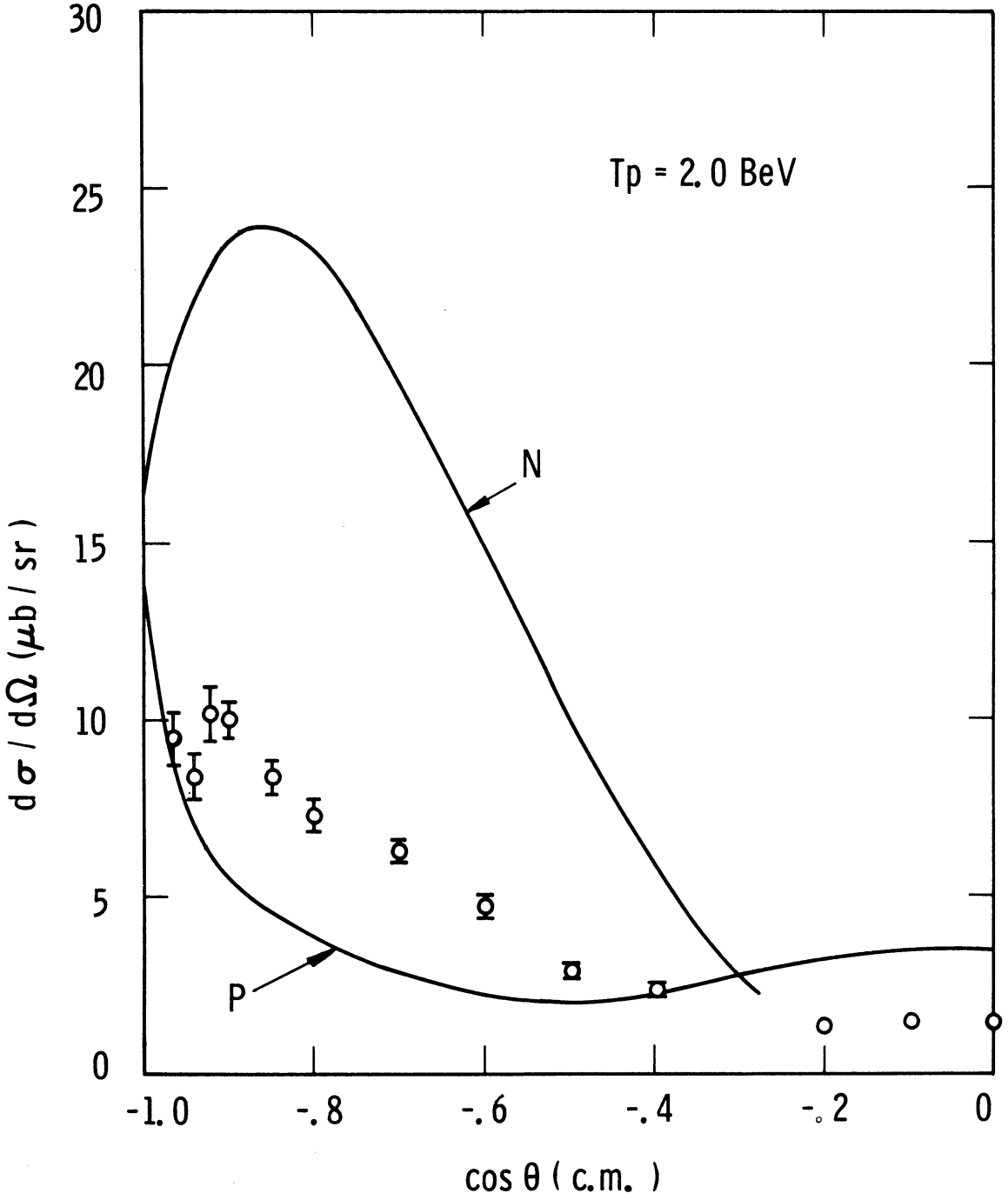

Fig. 8. One-nucleon exchange model (curve N) and one-pion exchange model (curve P) theoretical cross sections for the reaction $p+p \rightarrow d+\pi^+$ at an incident proton kinetic energy (T_p) of 2.0 BeV. The circles represent the data from this experiment.

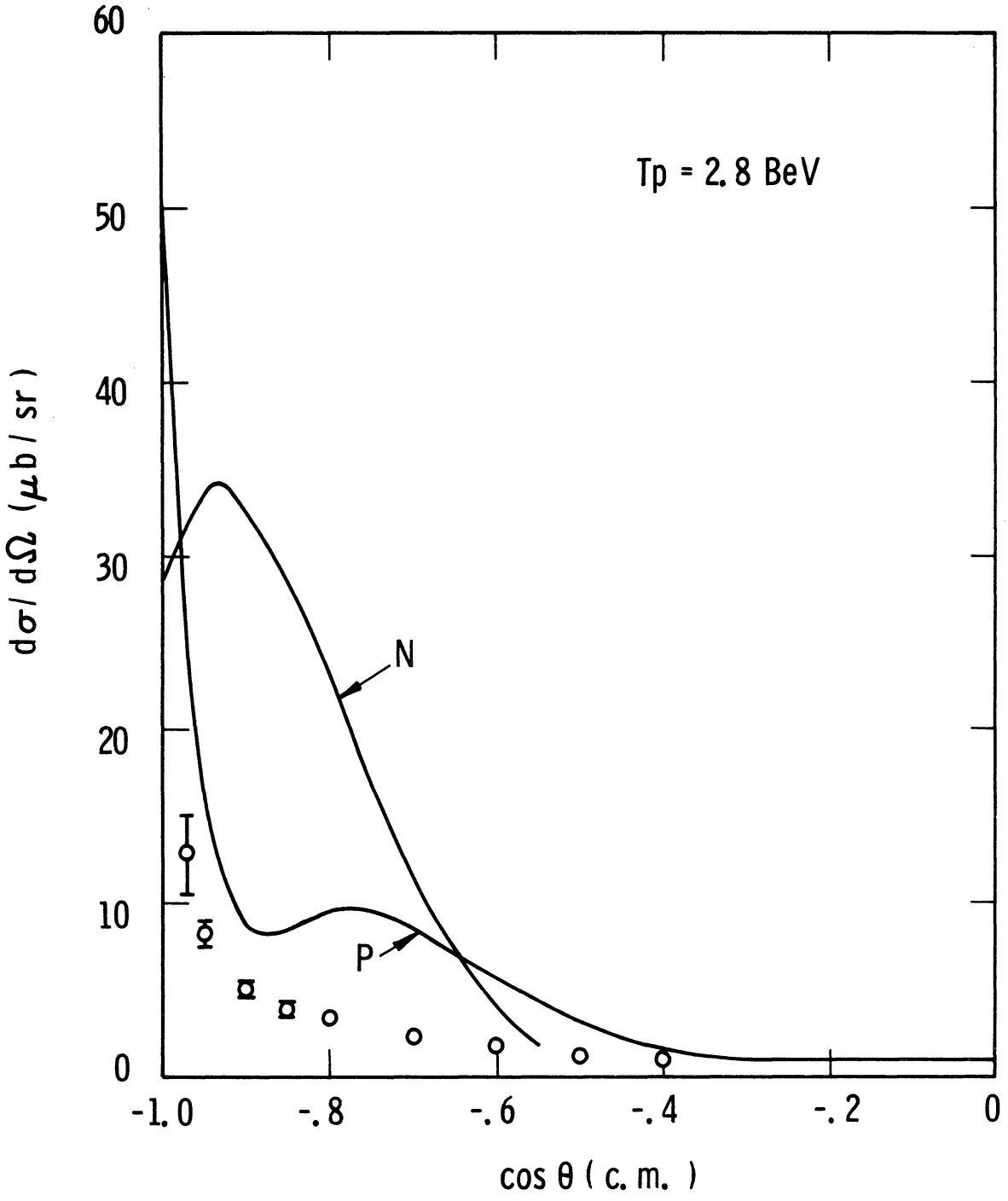

Fig. 9. One-nucleon exchange model (curve N) and one-pion exchange model (curve P) theoretical cross sections for the reaction $p+p \rightarrow d+\pi^+$ at an incident proton kinetic energy (T_p) of 2.8 BeV. The circles represent the data from this experiment.

Section B. The data from this experiment are given by circles in these four graphs. The conclusions which can be reached concerning the success of the various theoretical models as implied by the results of this experiment will be presented in Chapter VII.

The development of the one-nucleon exchange model as presented above should be considered as a first quantitative attempt to apply this model to the reaction $p+p \rightarrow d+\pi^+$. Improvements which can be made in the formulation include a better description of the deuteron wave function; the hard core should be replaced by a less drastic repulsive core, and the tensor interaction should be included. At the higher energies the deuteron should be treated relativistically. A more accurate treatment should be given to the effect of absorption, particularly since $d\sigma/d\Omega$ is quite sensitive to this. One should also include off-the-mass-shell effects for the exchanged nucleon and final state interactions, both of which have been neglected.

B. ONE-PION EXCHANGE MODEL

This model has been successful in interpreting single pion production in nucleon-nucleon interactions in the few BeV region.[35] For this reaction, however, the model is much more difficult to apply as there must be a final-state interaction between the nucleons to form a deuteron; as can be seen from the relevant Feynman diagrams shown in Fig. 2, this necessitates a loop integration. Yao[2] has made the

calculation, approximating the loop integration, and the following is a description of his calculation.

The R-matrix element for the π^+ exchange diagram can be written as

$$R_1=\left(\frac{1}{2\pi}\right)^4 \int d^4n_1 \left[\frac{-i\not{n}_1+M}{n_1^2+M^2-i\epsilon}\; i\sqrt{2}\; G\gamma_5 u(p_1')\right]^T \frac{-i\not{p}_2+M}{p_2^2+M^2-i\epsilon}$$

$$\left[A+i\not{q}B+i\not{r}C+\not{q}\not{r}D\right] u(p_1)\; \frac{1}{k_1^2+\mu^2-i\epsilon} \quad .$$

This expression contains four-vectors defined in the diagrams, expressions introduced in the previous section, and the quantity

$$M= A+i\not{q}B+i\not{r}C+\not{q}\not{r}D \quad .$$

Here $q=\frac{1}{2}(k_1+k_2)$, $r=\frac{1}{2}(k_1-k_2)$, and M is the most general expression for the unphysical pion nucleon scattering vertex (the right vertex in the Feynman diagrams), where A, B, C, and D are four invariant scalars. The other diagram can be incorporated into R_1 by straightforward isotopic spin considerations, the effect of which will be shown presently. Similar to the one-nucleon model, the total matrix element R is given by $R=R_1-R_2$ where R_2 is obtained by interchanging p_1 and p_1' in R_1.

By transforming the integration variable d^4n_1 to $dn_1^2 dp_2^2 dk_1^2 ds$, where $s=-(p_1+k_1)^2$, the n_1^2 and p_2^2 integrations are performed by assuming that the main contribution to these integrations comes from the region of the poles in the integrand at $n_1^2=-M^2+i\epsilon$ and $p_2^2=-M^2+i\epsilon$, and then extending the region of integration from $-\infty$ to $+\infty$. By also

assuming the integrand contains no other poles in the upper half plane (for either variable) and behaves well at infinity, the integrations can be performed in the complex plane, and are expressed in terms of the residues at these two poles. All quantities are now evaluated at $n_1^2=-M^2$ and $p_2^2=-M^2$. This assumption also simplifies the k_1^2 integration, since now, with $n_1^2=-M^2$, the width of the integration is $4i\alpha q_d$ (q_d is the magnitude of the three-momentum of p_1' in rest frame of the deuteron); since α is small quantity, the integration is approximated by $4i\alpha q_d$ times the integrand evaluated at the average value of k_1^2.

Since $p_2^2=n_1^2=-M^2$, one can easily show (by conservation of energy) that $\varkappa^2=-\alpha^2$ where $\varkappa$ is magnitude of the three-momentum of p_2 or n_1 in the deuteron rest frame. Thus the vertex function Γ, discussed in the previous section, is simply $\Gamma=\frac{4\pi N}{M}S$.

A final approximation is made by discarding the cross terms when the matrix element is squared, i.e. Yao takes $R^2\approx R_1^2+R_2^2$. After doing the spin sums the expression for the cross section becomes (neglecting deuteron D state)

$$\frac{d\sigma}{d\Omega}=\frac{2G^2}{4\pi}F^2(k_1^2)\frac{(2M-M_d)\alpha}{U^2}\frac{p_f}{p_i}\frac{k_1^2}{(k_1^2+\mu^2)^2}s\left[3\frac{d\sigma^+}{d\Omega}-\frac{d\sigma^-}{d\Omega}+3\frac{d\sigma^\circ}{d\Omega}\right]$$

$$+(p_1\leftrightarrow p_1').$$

$F(k_1^2)$ is the Ferrari-Selleri off-the-mass-shell correction for the exchanged pion, s is the c.m. energy of the virtual pion nucleon scattering process at the right hand vertex, and

$$\frac{d\sigma^{+}}{d\Omega} = \frac{d\sigma}{d\Omega}(\pi^{+}+p \rightarrow \pi^{+}+p)$$

$$\frac{d\sigma^{-}}{d\Omega} = \frac{d\sigma}{d\Omega}(\pi^{-}+p \rightarrow \pi^{-}+p)$$

and

$$\frac{d\sigma^{\circ}}{d\Omega} = \frac{d\sigma}{d\Omega}(\pi^{-}+p \rightarrow \pi^{\circ}+n).$$

These three cross sections are evaluated at c.m. energy s and the unique scattering angle at the right hand vertex corresponding to the angle of scattering of the deuteron. Thus the right hand vertex has been related to physical pion-nucleon scattering, and the linear combination of the three cross sections arises from considering both diagrams in Fig. 2.

Actually, Yao has included the effect of the deuteron D state in his calculation, which has a 12% effect, but in his final expression for $d\sigma/d\Omega$ he has neglected the $\frac{1}{1-\alpha\rho}$ term in N^2, which is 1.67. The theoretical cross section for this model has been evaluated at four incident proton energies, 1.35, 1.70, 2.07, and 2.8 BeV; these curves are shown in Figs. 6-9. The pion-nucleon scattering data necessary to make these numerical calculations were taken from references 36-39.

C. STATISTICAL MODEL

The basis of the statistical model is the assumption that in a collision process, all possible final states (states consistent with the conservation laws) have a probability of

of occuring which is proportional to the statistical weight for that state.[4] Thus the transition rates essentially depend only on the phase space factor, and not on the matrix element connecting the initial and final states. Hagedorn[5] has applied this model to any arbitrary two-body final state (pp initial state) and finds

$$\frac{d\sigma}{d\Omega}(\theta=90^\circ)=F(E)e^{-3.29E}$$

where θ is, for this reaction, the c.m. angle of the deuteron and E is the total barycentric energy. F(E) is proportional to the total pp inelastic cross section and another function of E, neither of which vary much with E. Thus one expects the energy dependence of the 90° differential cross section to be exp(-3.29E).

III. EQUIPMENT AND PROCEDURES

The external beam 2A from the Cosmotron, with an energy which varied from 1.0 BeV to 2.8 BeV, was brought through a magnet system consisting of one bending magnet, three quadrupoles, and two more bending magnets and focused on a three inch liquid hydrogen target. Desired events, which comprise 0.05% to 0.5% of the total pp cross section in this energy interval, were recorded when a coincidence occurred between the pion counter telescope and the deuteron counter telescope.

A. BEAM AND MAGNETS

The layout of the beam and magnets is shown in Fig. 10. The purpose of the 6" x 12" bending magnet H200 was to compensate for the fact that the angle at which the external beam leaves the Cosmotron depends on the beam energy. Thus, by adjusting the field of this H magnet, all of the beams were brought down the center of the ensuing quadrupole magnets. Another function of H200 was to collimate the beam; the vertical dimension of the beam was restricted to 1.5" by the pole pieces, while a collimator in the magnet gap provided horizontal collimation which varied from .75" to 2.0" depending on the beam energy. Collimation was necessary because of the joint requirement of small spot size (cross sectional area of the beam) and small angular divergence at the target, conditions which could not have been produced without collimation because of Liouville's Theorem.[40] The reason for this require-

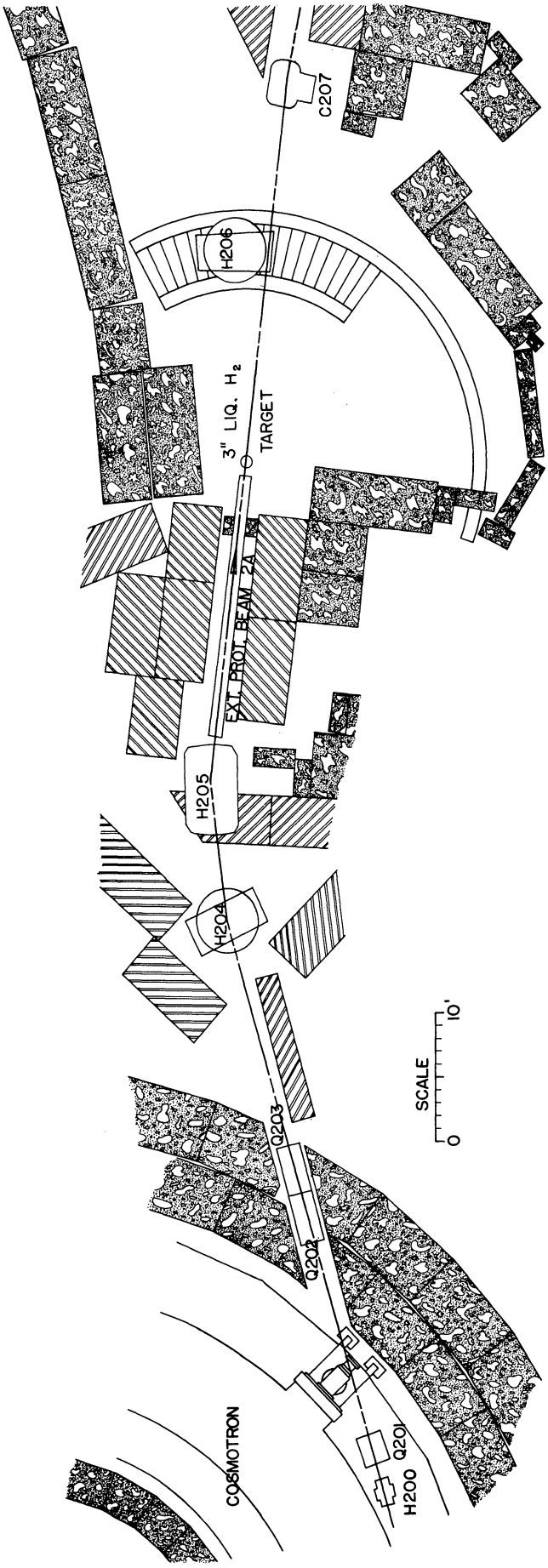

Fig. 10. The beam layout.

ment is that the beam spot size and divergence strongly influence the size of scintillation counters needed.

The beam was then focused at the target by the three 8" aperture quadrupole magnets Q201, Q202, and Q203. The currents in these magnets were determined with a beam-design computer program, and fine adjustments were made empirically by exposing polaroid films at the target and further downstream. The beam was designed to have a maximum spot size at the target of 1.5" and a maximum angular divergence of 1/5°.

The two bending magnets H204, with 12" x 60" pole faces, and the 18" x 36" H205 served to steer the beam through the center of the target at the desired angle in the horizontal plane. At the target the beam had a diameter of about 1" or 1.5", depending on the beam energy, and an angular divergence of about 1/10° in both the horizontal and vertical planes.

The C-magnet C207 merely served to bend the beam slightly so that the beam stop would not get in the way of counters D_3 and D_3' (see Fig. 11). Magnet H206 momentum analyzed the deuterons and will be discussed further in Section B.

Two direct methods were used to determine the energy of the beam. These methods were: 1) measuring the Cosmotron magnetic field and the radius of the circulating beam and 2) finding the frequency and orbital path length of the internal beam. These methods and formulas for applying them

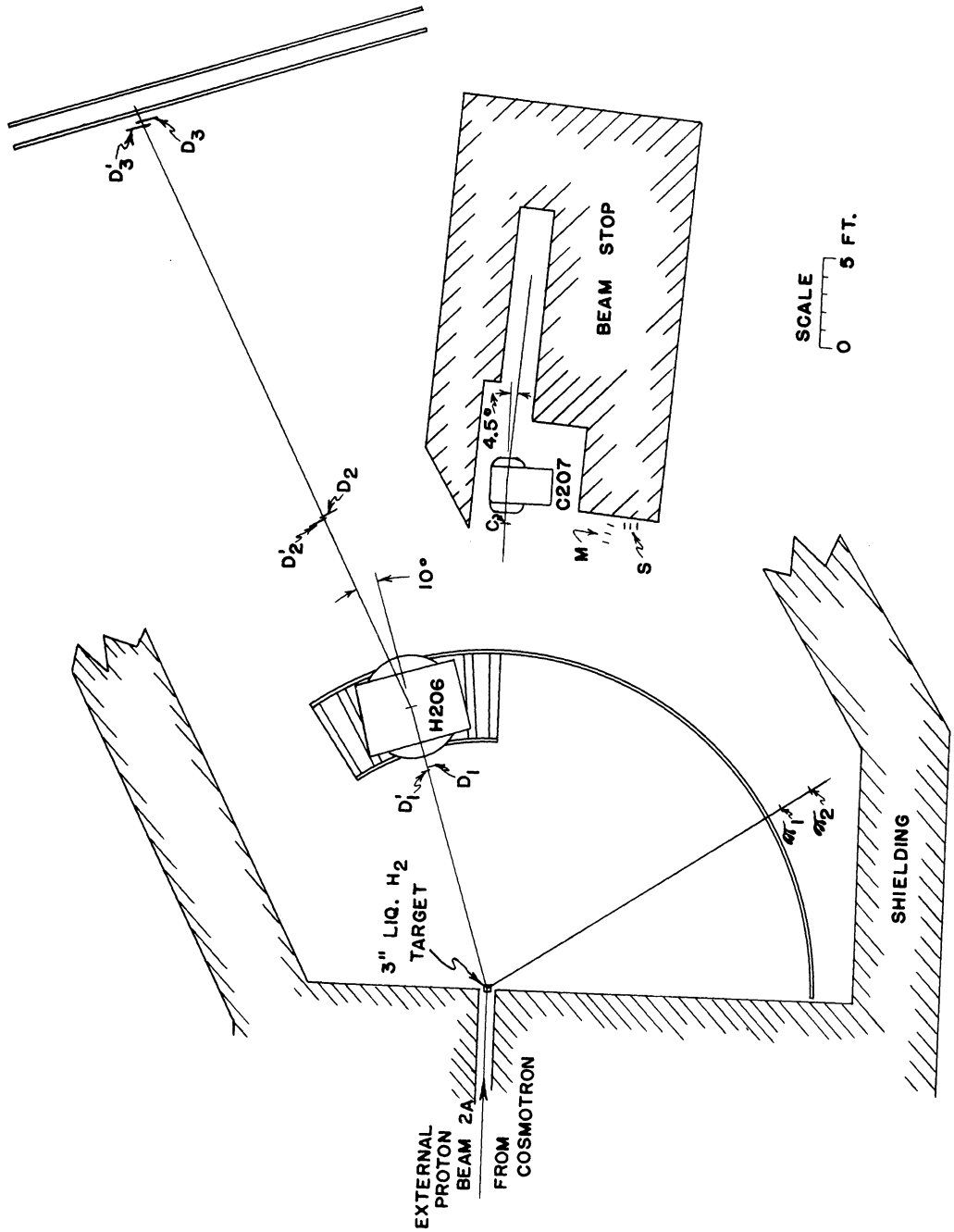

Fig. 11. The experimental layout

are described by Bennett.[41] A kinematical check on the beam energy was provided by the two deuteron scintillation counter telescopes (see Section B); if the beam did not have the energy corresponding to the angles at which the pion and deuteron telescopes were placed, there was an asymmetry of the number of good events arising from each of the two deuteron channels. These three methods together served to determine the beam energy to ± .05 BeV.

The beam rate, which was determined by requiring that the accidental rate (described in Chapter V, Section D) be less than 10% and that no counter have a singles counting rate greater than 2×10^5 counts/pulse, varied from 2×10^8 to 8×10^8 particles/pulse.

B. COUNTERS AND ELECTRONICS

A diagram of the experimental layout is shown in Fig. 11. The sizes of the counters are given in Table I. The first counter of the pion telescope, $\pi 1$, defined the solid angle which varied from 0.035 to 0.87 millisteradians depending on which of the two $\pi 1$ counters was used and its distance from the target, which varied from 8 to 20 ft. This distance could be changed by sliding the carriage upon which the π counters were mounted radially along a 6" wide-flange beam. The angle between the pion telescope and the beam was varied by rotating the wide-flange beam which pivoted on a post mounted directly underneath the target and rolled on a circular rail located 19' from the target. The pion angle, as well as the

TABLE I

SCINTILLATION COUNTER SIZES

Counter	Size width×height (in.)	Thickness (in.)
$\pi 1$	4×2	1/2
	or 2×1	1/2
$\pi 2$	7.5×4	1/2
D_1, D_1'	5.5×8	1/2
D_2, D_2'	13×19	3/8
D_3, D_3'	17×30	1/2
C	8 (diam)	1/2
M (3 counters)	1×1	1/4
S (3 counters)	1.5×1.5	3/8

deuteron angle, was determined quantitatively by calibrating a scale, mounted on this rail, using a transit secured to the top of the pivot post. (The transit can be seen in the bottom of Fig. 14.)

The deuteron was detected by two overlapping counter telescopes, consisting of three counters each, and an 18" x 36" bending magnet (H206 in Fig. 10 and Fig. 11) which deflected the deuterons by ± 10°. This magnet had a 10.5" separation between the pole faces. In Fig. 11 the two deuteron counter channels are labeled D_1, D_2, D_3 and D_1', D_2', D_3'. The flight path between the D_1 and the D_3 counters (40 feet) provided time-of-flight selection which when combined with the momentum selection from H206 separated the deuterons from pions and protons up to 2.4 BeV/c. Because the initial state of this reaction consists of identical particles, the differential cross section is symmetric about 90° in the center of mass and it was only necessary to measure it for deuterons going backward in c.m., where this momentum condition is satisfied. This region is shown in Fig. 12. Two deuteron channels were used to increase momentum resolution, to provide a kinematical check on the beam energy as described in Section A, and to insure that the deuteron telescope was located at the proper angle.

The deuteron angle was varied by moving the magnet, which was mounted on a carriage, along the arc of a circle on railroad tracks (see Fig. 11). The D_1 and D_2 counters were at-

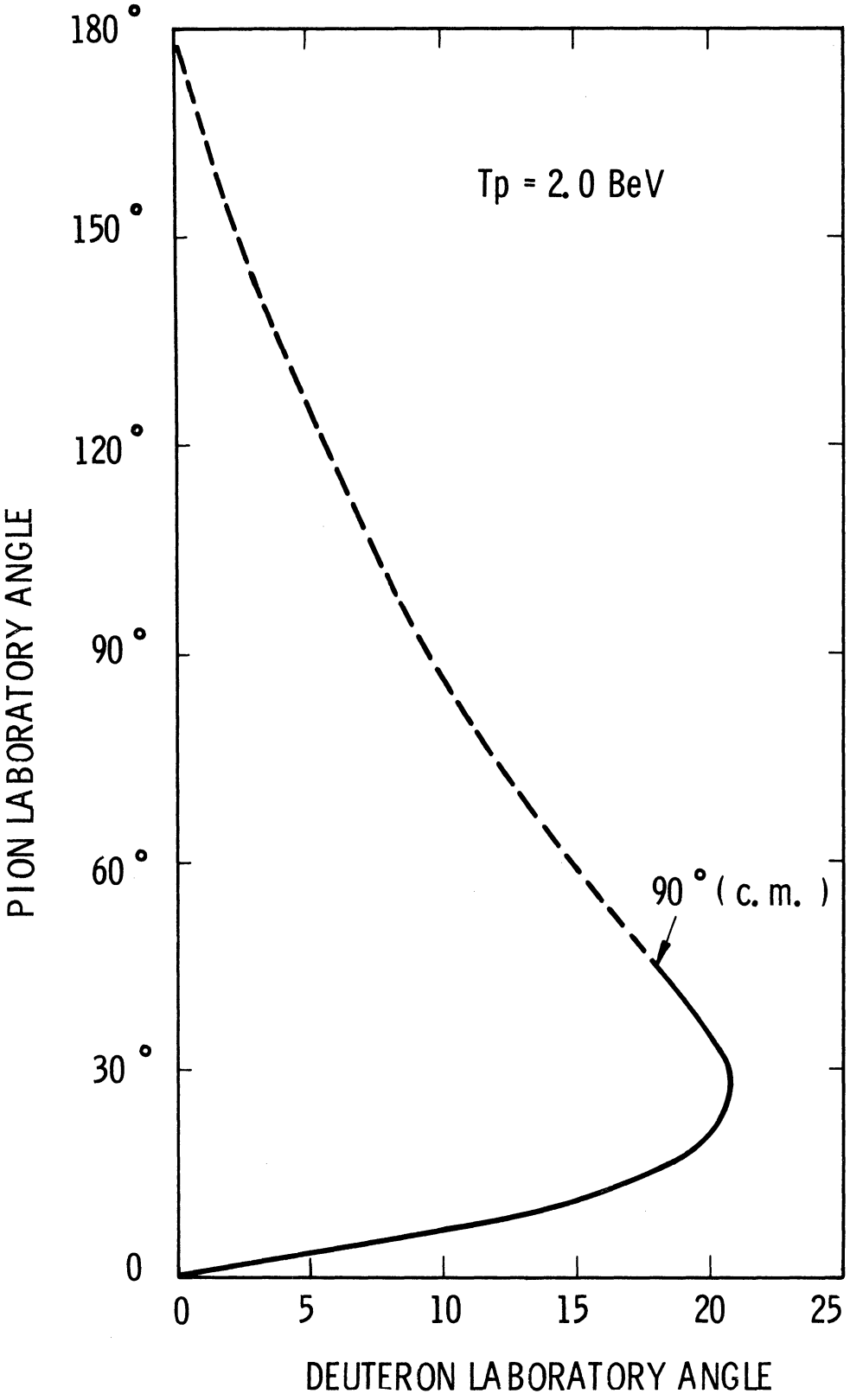

Fig. 12. Kinematics curve for the reaction $p+p \rightarrow d+\pi^+$ at an incident proton kinetic energy (T_p) of 2.0 BeV. The solid line represents the region where the cross sections were measured in this experiment, and corresponds to deuterons going backward in the barycentric system.

tached to the magnet carriage while the D_3 counters could be moved along a pair of parallel I-beams. The magnet was calibrated by using the standard wire-orbit technique.[42]

It was possible to reduce the size of the D_3 counters by approximately 20% by taking advantage of kinematical focusing. If p and φ are the laboratory momentum and angle of the deuteron, then $dp/d\varphi>0$ as φ goes from 0° to its maximum, for deuterons backward in c.m. (see Fig. 12), and then $dp/d\varphi<0$. By bending the deuterons counterclockwise (as seen from above) in the first case and clockwise in the second, this effect serves to focus the deuterons. The sizes of the deuteron counters were determined by an IBM 7090 computer program which, using ray tracing techniques, considered the effects of the beam size and angular divergence, πl size and distance from the target, the length of the target, multiple Coulomb scattering, and kinematical focusing. The amount of overlap between pairs of deuteron counters was determined primarily by considering the Coulomb scattering of the deuterons.

The kinematics of the reaction (see Fig. 12) are such that it was possible to measure all barycentric deuteron angles θ for $0 \geq \cos\theta \geq -.96$ or $-.97$ (depending on beam energy) by varying the π telescope angle from 5° to 58° and the deuteron telescope from 6.7° to 23°. At small laboratory deuteron angles the beam struck the yoke of H206 and it was necessary to reduce the beam intensity so that the singles counting rates in the D_1 counters would not be too large.

The beam was monitered by two sets of scintillation counter telescopes containing three counters each. The M moniter telescope, used to normalize the measured cross sections, was pointted toward the target at a laboratory angle of 11.3° while S was aligned so that it looked at counter C (see Fig. 11). The C counter was located in the beam 20 feet downstream from the target and served as a source of particles for S which essentially depended only on the incident beam intensity and not upon whether the target was full or empty, since less than 2% of the beam interacted in the liquid hydrogen. This counter was also used to indicate the beam spill. (The beam spill refers to the time distribution of the beam particles.) The calibration of M is discussed in Chapter IV; the purpose of S was to determine the beam intensity when the target was empty (see Chapter V, Section E).

Before the experiment all of the scintillation counters were plateaued and the characteristic time delay between the incidence of a particle and the output pulse from the RCA 6810 photomultiplier tubes was determined with a light pulser. During the experiment these delays were checked by running time-of-flight delay curves on protons from elastic scattering. With this information, it was possible to calculate the proper delay cables to insert between the counters and coincidence circuits for the $\pi^{+}d$ final state. Both D_3 counters had a phototube on each end to decrease the timing jitter and increase the signal to noise ratio from these counters. All counters

except the M moniter counters had plexiglas light pipes to transfer the light from the scintillator to the phototube. A pulse from the Cosmotron was used to generate a gate signal which was adjusted to turn the scalars on during the desired portion of the beam spill.

A block diagram of the electronics is shown in Fig. 13. The logic circuits are standard units described in detail by Sugarman et al.[43] The 10Mc scalars were manufactured by the Transistor Specialties Inc. The πD coincidence is a coincidence between the π telescope and either (or both) of the deuteron telescopes. The accidental coincidences, called πD̄, will be discussed in Chapter V, Section D. The scalars πD° and πD' show how many good events arise from each channel.

C. HYDROGEN TARGET

A photograph of the hydrogen target is shown in Fig. 14. The upstream beam pipe is visible behind the target. The beam enters the vacuum chamber in which the target is enclosed through a .010 in. mylar window. The liquid hydrogen is contained in the .010 in. mylar bag located in the upstream end of the vacuum chamber. This bag is 3 in. long and 4 in. in diameter and is supported from above by the gravity filling pipe which is attached to a 1 in. wide metal ring which surrounds the target. The exhaust pipe is connected to the bottom of this ring. Thermal insulation for the liquid hydrogen is provided by wrapping the mylar bag with 20 layers of .00025

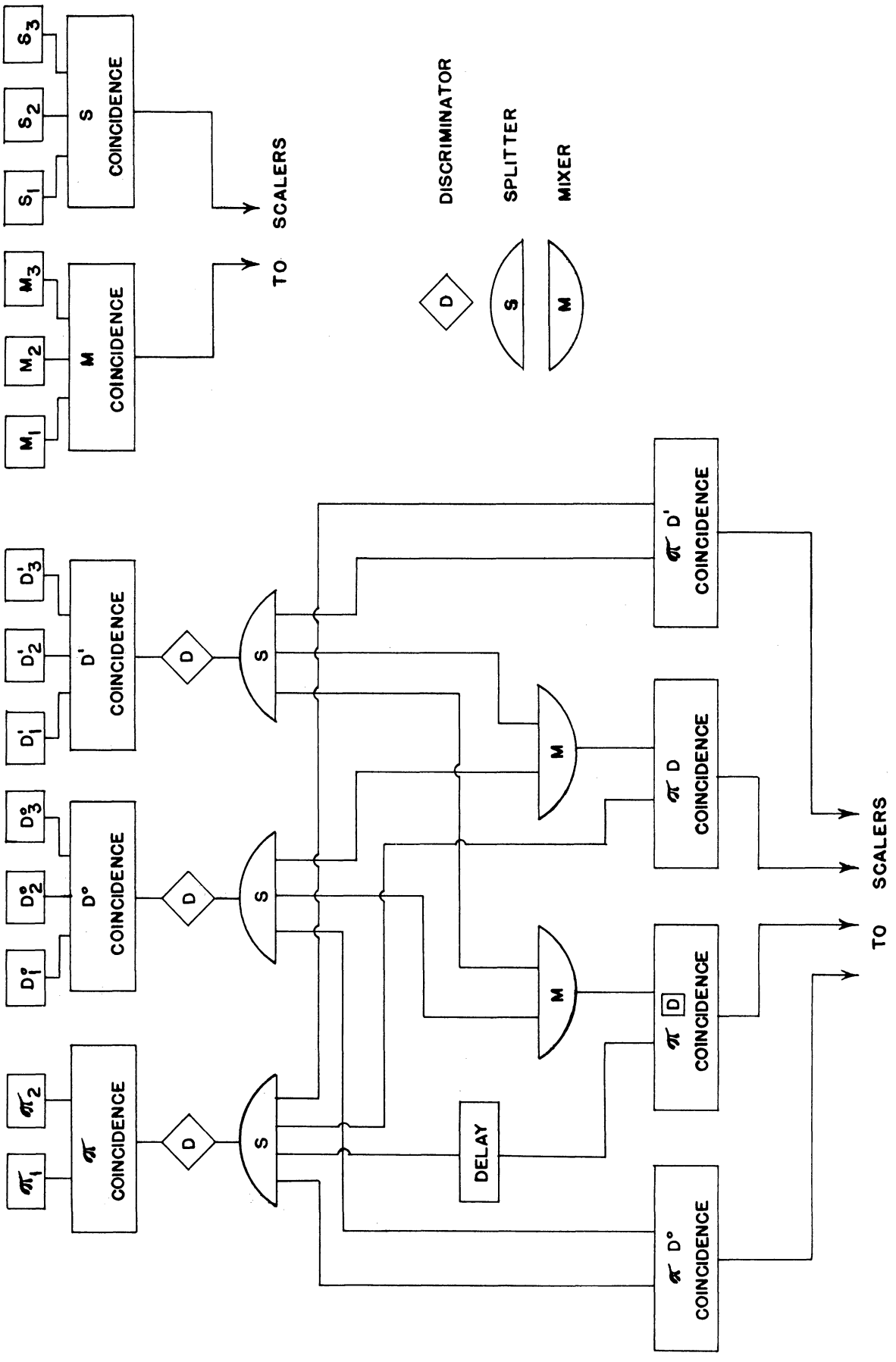

Fig. 13. A block diagram of the electronics.

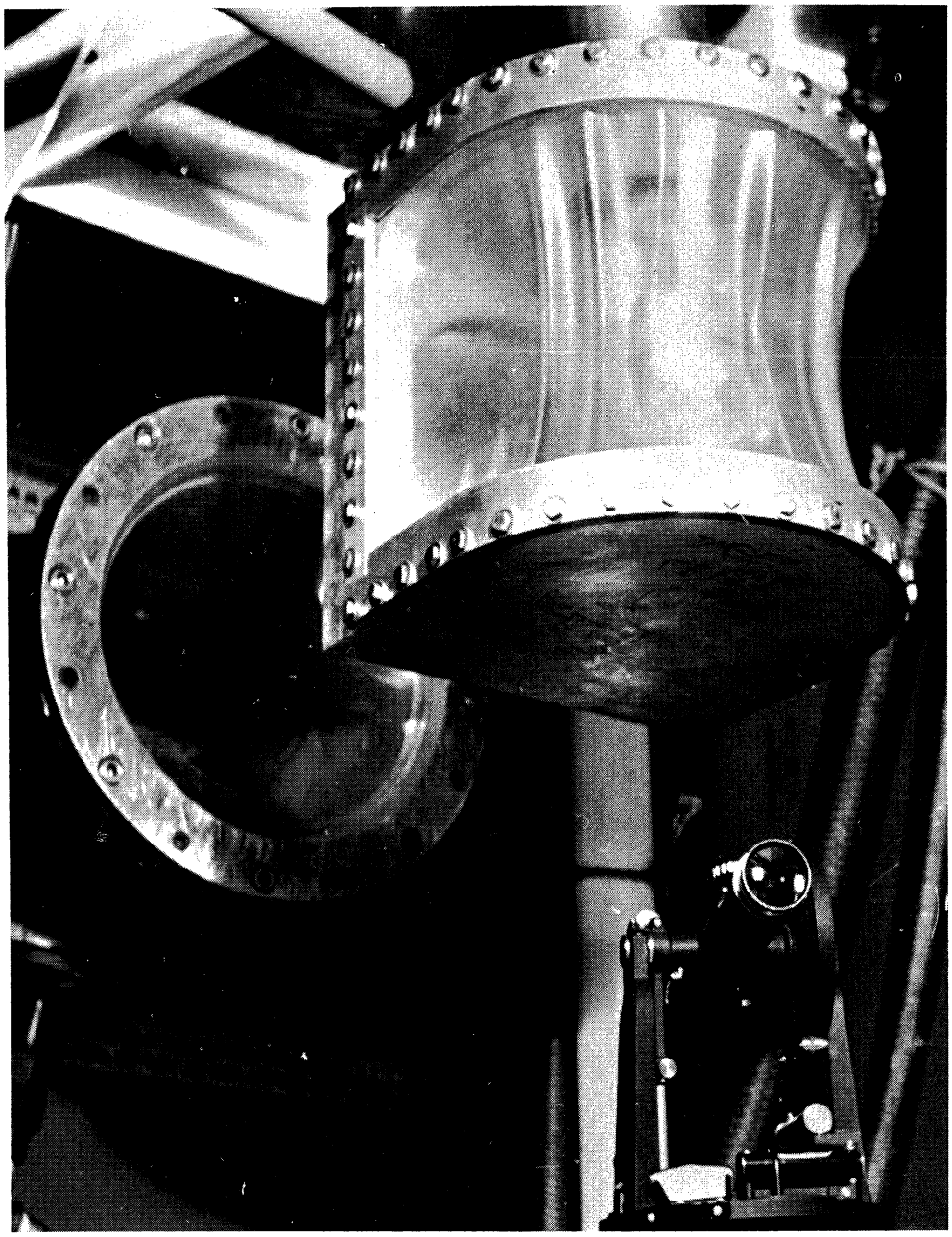

Fig. 14. The liquid hydrogen target.

in. aluminized mylar and a layer of aluminum foil, and by the surrounding vacuum. As can be seen in the photograph, the vacuum chamber is designed so that the emerging pions and deuterons which were recorded passed through a .015 in. mylar window.

D. EXPERIMENTAL CHECKS

Numerous checks were made to verify that the events detected indeed corresponded to the π^+d final state. Deuteron time-of-flight delay curves, obtained by varying the delay between the π and D coincidence circuits (see Fig. 13), resulted in yield versus delay curves which typically had a flat top of width 7 nsec, a full width at half maximum of 10 nsec, and a full width for a 10% yield of 16 nsec. These curves were centered about the delay corresponding to the π^+d final state. Curves of yield versus the current in magnet H206 similarly had a maximum at the current corresponding to the momentum of the deuteron from the π^+d final state; these curves had a full width at half maximum of 75 amps and dropped rapidly to zero. Angular correlation measurements, obtained by fixing the deuteron (pion) angle and finding the yield as a function of pion (deuteron) angle also identified the π^+d final state; of course, the shape of these curves depended strongly upon the kinematical region in which they were taken (note Fig. 12). A curve of yield versus pulse length in the deuteron channels was run to insure that no events were lost because of the spread in deuteron flight time being of the

order of the time resolution of the πD coincidence unit. Finally, for low beam energies it was possible to measure the differential cross section at forward barycentric deuteron angles and verify the symmetry of the reaction about 90°.

IV. NORMALIZATION

The moniter counters M were calibrated by measuring the C^{11} activity induced by the beam in .004 in. thick polyethylene foil by means of the reaction $C^{12}(p,pn)C^{11}$. The foil was mounted on the downstream end of the target assembly and irradiated for one minute by a beam with an approximate intensity of 2-5 x 10^9 particles/pulse. The C^{11} activity was then measured in a NaI well- counter by detecting one or both of the gamma rays resulting from the annihilation of the positrons emitted by the C^{11} atoms.

If the foil were irradiated by a continuous beam of protons, then the number of C^{11} atoms present, N(t), would be determined by

$$\frac{dN(t)}{dt} = -\lambda N(t) + \frac{\sigma}{A} C\varphi$$

where λ is the C^{11} decay constant, σ is the $C^{12}(p,pn)C^{11}$ cross section, A is the foil area, C the number of C^{12} atoms in the foil (assumed constant), and φ is the beam rate. Thus, after irradiation for t_1 minutes,

$$N(t_1) = \frac{\sigma C}{A\lambda}(1-e^{-\lambda t_1})\varphi$$

or

$$N(t_1) \approx \frac{\sigma C}{A} F\left(1-\frac{\lambda t_1}{2}\right)$$

where $F=\varphi t$ is the total number of protons passing through the foil during t_1, and λt_1 is a small quantity ($\lambda t_1 = 3.4 \times 10^{-2}$ for t_1=1 min.). If φ is taken to be a series of equally spaced impulse functions instead of a constant, corresponding more closely to the actual physical situation, the same expression

for $N(t_1)$ is obtained to first order in λt_1. F can then be determined by this equation.

σ has been measured at 1.0 BeV by Poskanzer et al.[44] and at 2.0 BeV and 3.0 BeV by Cumming et al.[45] These authors report $\sigma=26.6 \pm 1.3$ mb at 1.0 BeV, $\sigma=26.0 \pm 0.9$ mb at 2.0 BeV, and $\sigma=26.6 \pm 1.0$ mb at 3.0 BeV. To obtain σ for the energies of this experiment it was usually necessary to interpolate. Since polyethylene has a chemical formula $(CH_2)_n$, $C=N_0W/14.0$ where N_0 is Avogadro's number and W, the weight of the foil, is determined with an analytical balance. The 1.1% occurrence of C^{13} in natural carbon isotopes introduces no error in the analysis since the cross sections quoted above were based on the total carbon content, not just the C^{12}. $N(t_1)$ is obtained by measuring N_{ab}, the number of C^{11} decays during the period t_a to t_b in a well counter. Then since

$$N_{ab}=\int_{t_a}^{t_b} \lambda N(t)dt$$

and

$$N(t)=N(t_1)e^{-\lambda(t-t_1)} \text{ for } t>t_1$$

it follows that

$$N_{ab}=N(t_1)e^{\lambda t_1}(e^{-\lambda t_a}-e^{-\lambda t_b}).$$

Usually $N(t_1)$ was determined in this manner by counting the foils for six one minute intervals and taking the average of the six resulting $N(t_1)$'s. However, before F can be computed, it is necessary to apply a correction to $N(t_1)$ obtained in this manner. When the C^{11} atoms are produced,

they possess enough kinetic energy to allow a breaking of chemical bonds and the subsequent formation of gaseous molecules which can diffuse out of the foil. This "hot atom" loss, described by Cumming et al.[46], is found to be about 14.2% for .004 in. polyethylene foil by Cumming et al.[47]

The standard error in calculating F in this fashion arises primarily from the error in σ, the statistical error in N_{ab}, and the fact that the efficiency of the N_aI well-counter is only known to within ± 5.0%. The result of combining these errors orthogonally is about ± 8%.

The calibration of the moniter counters M is given by F/M, where M is the number of coincidences in the moniter counters while the foil is irradiated by F protons. For most energies two foils were irradiated, and the resulting F/M values always agreed to within 3%. An exception occurred, however, at the end of the experiment when the calibration factor F/M was remeasured at a previous energy, 2.0 BeV, and differed from the previous calibration by 7%; however, it was discovered in a subsequent experiment that for some runs the beam scraped a beam pipe upstream of the target, resulting in an abnormally high M reading. This introduced no error, since each run had a separate calibration factor F/M which was accurate, within the 8% error mentioned above, for that run.

V. DATA CORRECTIONS

This section describes the corrections which were applied to the data.

A. NUCLEAR INTERACTIONS

Some of the desired events were not recorded because the pi and/or the deuteron did not travel completely through their respective telescopes because of nuclear scattering in the hydrogen target, air, or scintillators. The number of events lost in this manner can be calculated if the relevant cross sections are known. A good approximation to the actual cross sections is the geometric cross section, defined by $\sigma_g=\pi r_n^2$ where $r_n \approx r_o A^{1/3}$ is the nuclear radius, A the mass number of the material and r_o a constant. This formula can be improved by remembering that in the particle energy region we are dealing with, a nuclear collision can be thought of as occurring between the incoming particle and the individual nucleons of the nucleus.[48] Since the pion and deuteron collision cross sections are experimentally known for neutron or proton targets, the collision cross sections for other materials can be approximated by multiplying the corresponding geometric cross section by the ratio of the pion-nucleon (or deuteron-nucleon) empirical cross section to the geometrical cross section for A=1. Thus σ_{DA}, the total cross section for deuterons on material with mass number A, is given by $\sigma_{DA}=\sigma_{DN}A^{2/3}$ where σ_{DN}, the deuteron-nucleon total cross section, is approximately 80 mb.[49] Similarly, $\sigma_{\pi A}=\sigma_{\pi N}A^{2/3}$

where $\sigma_{\pi N}$=35 mb.[50] For pion energies below 1 BeV, $\sigma_{\pi N}$ is taken to be the average of the pion-neutron and pion-proton cross sections. This refinement of the geometric cross section is necessary because the deuteron is quite unstable in matter, and interacts much more strongly than the geometric cross section would indicate.

B. MULTIPLE COULOMB SCATTERING

As discussed previously, the experiment was designed so that there would be no loss due to Coulomb scattering. It was possible to verify this experimentally in the following manner: at one pion angle at each energy, the differential cross section was measured twice, once using a pion counter which subtended the designed solid angle and once with a solid angle one-fourth as large. If the deuteron counter telescope were not large enough to collect all of the desired deuterons, the yield would be higher with the smaller pion solid angle since then the deuterons would be confined to a smaller region. There was no statistically significant difference between the two measurements.

Obviously one cannot prevent pion Coulomb scattering loss by increasing the pion counter sizes since one of the pion counters defined the solid angle. However, there are approximately as many pions scattered into the system as there are scattered out so there is no net effect providing the deuterons corresponding to the pions which scatter into the system are collected by the deuteron telescope. That this

was actually true was shown experimentally by the results of the test described in the previous paragraph.

C. DECAY OF PIONS

The pion is unstable, decaying into a muon and a neutrino with a mean life of 25.5 nsec.[51] The variable pion path length, which had a maximum value of 22 feet, required a maximum of 23 nsec (4.5 nsec in the pion barycentric system) flight time. Thus as many as 16% of the pions decayed before reaching the final counter. However, the muons were emitted by the highly relativistic pions in a narrow forward cone with a maximum half-angle of 3.0° in the laboratory. Thus the coincidence was completed in many cases by the muons, while events lost by the muon missing the pion counters were compensated for by pions which were slightly off angle being counted by decaying and sending a muon through the counter system.

Verification that the number of events lost by pion decay was not significant was done empirically by remeasuring one point with a 50% shorter pion travel length. There was no statistically significant difference in the two resulting cross sections.

D. ACCIDENTAL COINCIDENCES

Accidental events, in which independent pulses from the pion and deuteron channels occur by chance within a short time interval and are counted by the coincidence circuit,

were indicated by recording the coincidences between the two channels when they were 31 nsec out of time. These "out-of-time" coincidences, $\pi\mathbb{D}$ in Fig. 13, were recorded throughout the experiment; they obviously were not exactly equal to the number of accidentals included in the good events and in subtracting them from the good events this statistical uncertainty is reflected in the statistical error (see Chapter VI). By adjusting the beam intensity, the accidentals were always held to less than 5% of the good events; however, the structure of the beam spill, which could not be controlled, was much more influential in causing accidentals than the beam intensity was.

E. BACKGROUND EVENTS FROM TARGET

When the liquid hydrogen was emptied from the target, the number of events recorded could be expressed as a fraction of the number of events with a full target for the same amount of incident beam by using the S moniter counters. The distribution of the target empty to target full ratio was approximately Gaussian, centered about 2.7%. Approximately 1.3% should be expected from hydrogen in the mylar serving as a target. The number of events arising from the hydrogen vapor which remains in the target after it is emptied is about .1% while the rest can be attributed to quasi-events in which the target protons were in the nuclei of carbon atoms in the mylar. Thus, this effect was corrected in the data by subtracting 2.6% from the good events, where, of

course, the hydrogen vapor events should not be subtracted since the vapor is not present when the target is full.

F. BEAM ATTENUATION

Since part of the beam interacts in passing through the target, the downstream end of the target only sees some fraction of the initial beam flux. This effect can be corrected by using an effective target length, L_{eff}, which is defined by

$$I(o)L_{eff}=\int_{o}^{L} I(x)dx$$

where L is the actual target length and I(x) is the number of protons per pulse which pass through x, the x axis pointing along the beam direction with its origin at the upstream edge of the target. The resulting expression L_{eff} is

$$L_{eff}\approx L(1-\frac{\sigma\rho L}{2})$$

where σ is the total pp cross section and ρ the number of protons per cubic centimeter in the target.

G. COUNTER DEAD TIME

The dead time of a counter, τ, can be defined as the time between the traversal of an ionizing particle and the time when the counter has recovered enough to record another ionizing particle, giving an output pulse large enough to be detected by the subsequent electronics. Thus, if the beam has a spill time T and the counting rate in a counter is S counts per pulse, the fraction of T that the counter cannot record pulses is $S\tau/T$. For example, if $S=10^5$ counts

per pulse, τ=10 nsec and T=100 msec, $S\tau/T$=1%. However, since the beam has structure (i.e. the time distribution of beam particles is not a square wave) more than 1% of the desired events could be lost since they are more likely to occur during the period when the counter has its highest counting rate. Another difficulty in making this correction is that during the experiment the counting rates in the counters were not continuously monitered and are known only approxmately. The counter dead time data correction was made using the above technique and the uncertainties involved are reflected in the systematic error (see Chapter VI).

H. BEAM ENERGY

As mentioned previously, the energy of the beam could be determined with an accuracy of about ± 0.05 BeV. In addition to the fact that the energy at which the cross section is measured is unknown by this amount, there is an error introduced of approximately ± 2% in transforming the measured laboratory cross sections to the barycentric cross sections, since the Jacobian for a given laboratory angle is a function of the beam energy. This effect of course cannot be corrected for.

I. COUNTER EFFICIENCY

Because of the small size and relatively large thickness of the π counters and the D1 counters (see Table I), it is assumed that they were essentially 100% efficient. The

efficiencies of the D2 and D3 counters were not measured, but were estimated to be 99% ± 1% because of the moderate size of the D2's and the fact that each D3 counter had two photo-tubes.

VI. RESULTS

The following formula was used to calculate the differential cross sections:

$$\frac{d\sigma}{d\Omega} = \frac{\pi D - \pi \mathbb{D}}{\rho \frac{F}{M} MLJ(\Delta\Omega)} \alpha\beta\gamma\delta\epsilon\zeta,$$

where πD = total number of events at a given angle

$\pi \mathbb{D}$ = total number of accidental events at a given angle

ρ = density of liquid hydrogen = $4.23\ 10^{22}$ protons/cc

$\frac{F}{M}$ = normalization factor for M moniter telescope, typically $3 \cdot 10^6$

M = number of coincidences in M telescope

L = length of hydrogen target when filled with liquid hydrogen and surrounded by vacuum=3.03 in.

$\Delta\Omega$ = solid angle subtended by πl counter in the laboratory

J = Jacobian which transforms solid angle ($\Delta\Omega$) from laboratory to c.m.

α = correction for nuclear interaction = 1.13 ± .03

β = correction for multiple Coulomb scattering loss= 1.01 ± .01

γ = correction for background events = .974 ± .01

δ = beam attenuation correction = 1.01

ϵ = correction for counter dead time= 1.03 ± .03

ζ = correction for counter efficiency = 1.02 ± .02

$\alpha\beta\gamma\delta\epsilon\zeta$ = total correction = 1.18 ± .05.

The errors stated in the corrections applied above are estimated. When combined orthogonally with the Jacobian error of ± 2% due to the uncertainty of the beam energy and the normalization error of ± 8%, the net non-statistical error is ± 10%. The statistical error, which is determined by the expression $\sqrt{\pi D+\pi\bar{D}}/(\pi D-\pi\bar{D})$, ranged from about ± 5% to ± 15% but was usually about ± 7%.

The results are shown in Table II and Figs. 15-21, where the error bars indicate the standard deviation from counting statistics. The total cross sections are given in Table II and in Fig. 22; they were obtained by fitting the differential cross sections with a series of even powers of $\cos\theta$, using a weighted least squares method, and integrating the resulting expression analytically. The vertical error bars represent statistical errors, while the horizontal error bars indicate the uncertainty of the beam energy. Figs. 15-22 also show the other existing experimental data.

Preliminary results of this experiment were reported at the International Conference on High Energy Physics at Dubna, U.S.S.R. (1964) and published in Physical Review Letters.[52]

Table II

DIFFERENTIAL AND TOTAL CROSS-SECTIONS FOR THE REACTION $p + p \rightarrow d + \pi^+$

(T_p is the kinetic energy of the incident proton. E* is the total energy of the c.m. system. θ is the c.m. angle of the deuteron relative to the direction of the incident proton.)

		$d\sigma/d\Omega$, $\mu b/sr$ (c.m.)						
Cos θ (c.m.)	T_p (BeV):	1.0	1.3	1.5	1.7	2.0	2.5	2.8
	E* (BeV):	2.3	2.4	2.5	2.6	2.7	2.9	3.0
-.97							12.3±1.2	12.8±2.3
-.965				9.9± .8	10.6± .9	9.5± .7		
-.96		50.1±2.5						
-.95			17.5±1.3	12.1± .7	12.5± .9		10.6 ± .8	8.3± .5
-.94						8.3± .6		
-.93		49.9±2.7						
-.925			22.7±1.6	14.6±1.0	14.6± .7		6.4±1.0	
-.92						10.2± .7		
-.90		52.1±2.0	21.0± .8	15.9± .6	16.1± .8	10.0± .5	5.7± .4	5.1± .4
-.85			24.2±1.1	16.4± .6	12.9± .9	8.4± .5		3.7± .3
-.80		51.2±2.4	25.0± .9	13.3± .8	11.9± .8	7.3± .4	3.5± .2	3.3± .3
-.70		45.9±2.2	23.8± .8	13.1± .7	9.4± .5	6.2± .3	2.7± .3	2.2± .2
-.60		42.1±1.5	20.1± .7	10.2± .5	6.0± .4	4.7± .3	1.9± .2	1.7± .2
-.50		33.4±1.7	17.8± .9	9.7± .5	5.0± .3	2.9± .2	1.4± .1	1.2± .1
-.40		31.9±1.6	14.5± .7	7.6± .3	4.4± .2	2.4± .1		1.0± .1
-.30		24.4±1.2	13.6± .7	8.6± .5	3.8± .2		.7± .1	
-.20		23.5±1.1	12.4± .6	6.9± .5	3.1± .2	1.3± .1		
-.10		21.0± .9	13.0± .7	6.2± .4	3.0± .2	1.2± .1	.8± .1	
0		20.3± .9	12.2± .6	6.3± .4	2.9± .2	1.1± .1		
σ_{total} (μb)		452±21	217±11	123±7	84±5	53±3	33±3	30±3

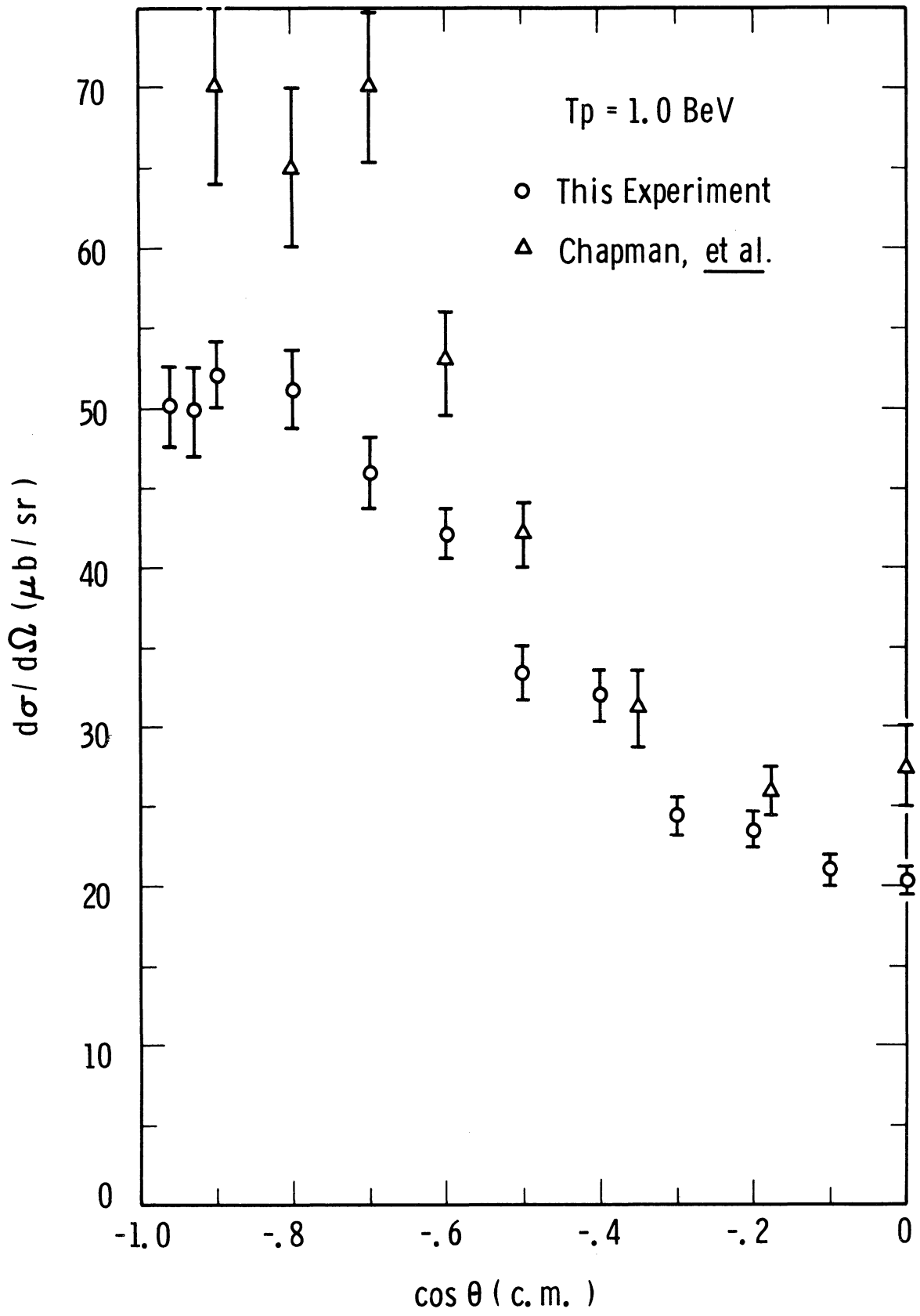

Fig. 15. Center of mass differential cross sections for the reaction $p+p \rightarrow d+\pi^+$ versus the cosine of the barycentric scattering angle at an incident proton kinetic energy of 1.0 BeV. The data shown are from this experiment and from Chapman *et al.*[12]

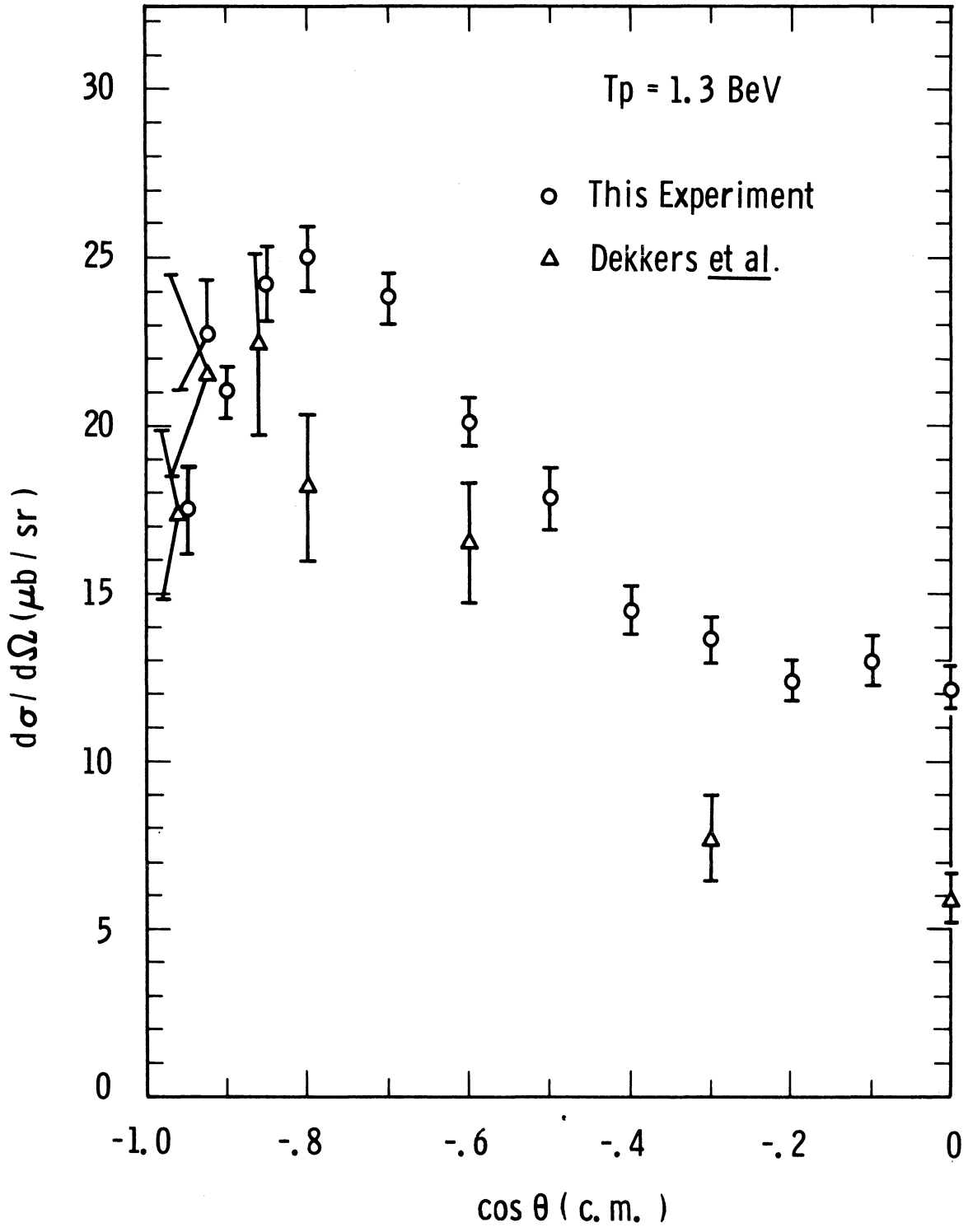

Fig. 16. Center of mass differential cross sections for the reaction $p+p \rightarrow d+\pi^+$ versus the cosine of the barycentric scattering angle at an incident proton kinetic energy of 1.3 BeV. The data shown are obtained from this experiment and deduced from the $\pi^+ + d \rightarrow p+p$ experiment of Dekkers *et al.*[15]

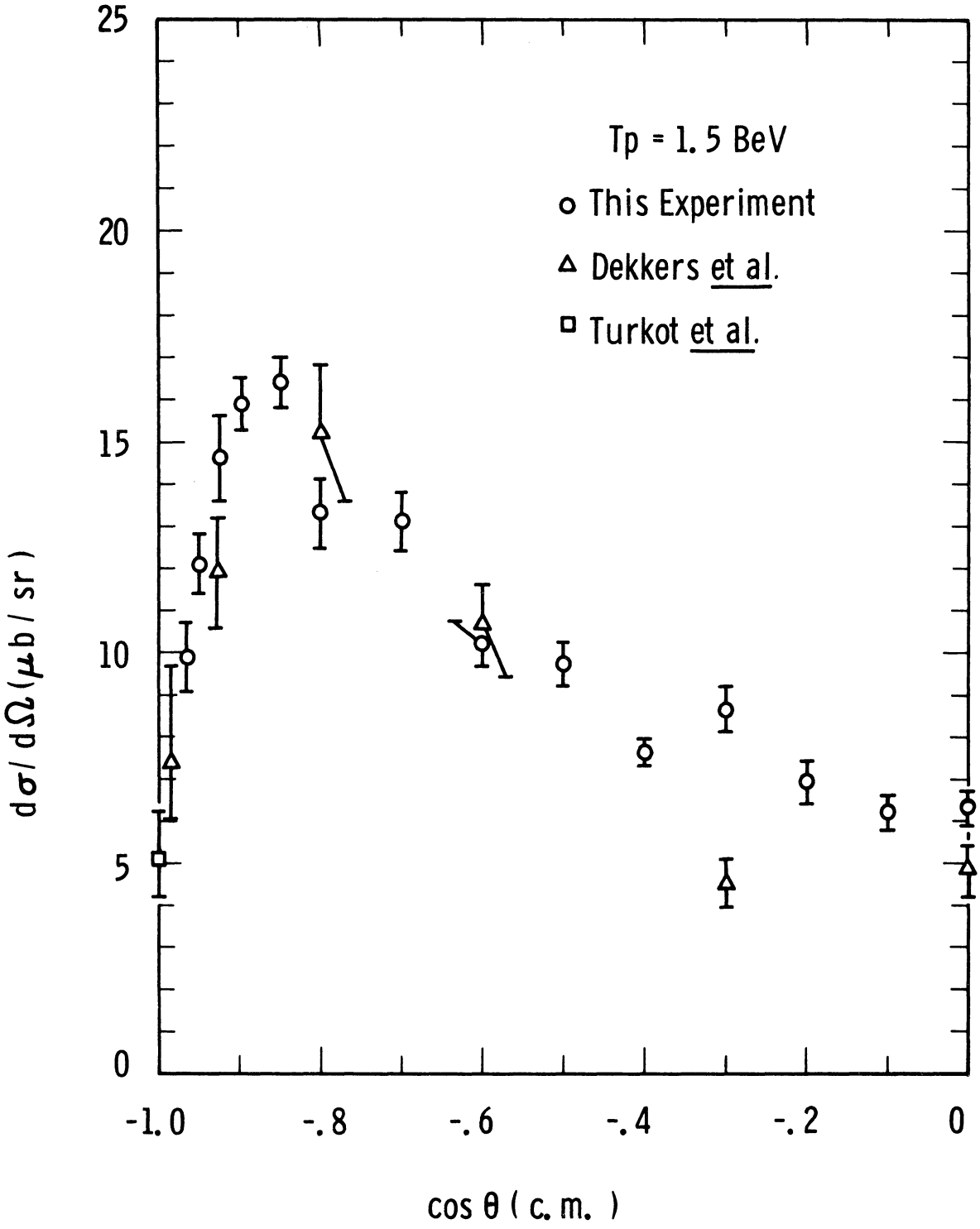

Fig. 17. Center of mass differential cross sections for the reaction $p+p \rightarrow d+\pi^+$ versus the cosine of the barycentric scattering angle at an incident proton kinetic energy of 1.5 BeV. The data shown are obtained from this experiment and from Turkot et al.[6] and deduced from the $\pi^+ + d \rightarrow p+p$ experiment of Dekkers et al.[15]

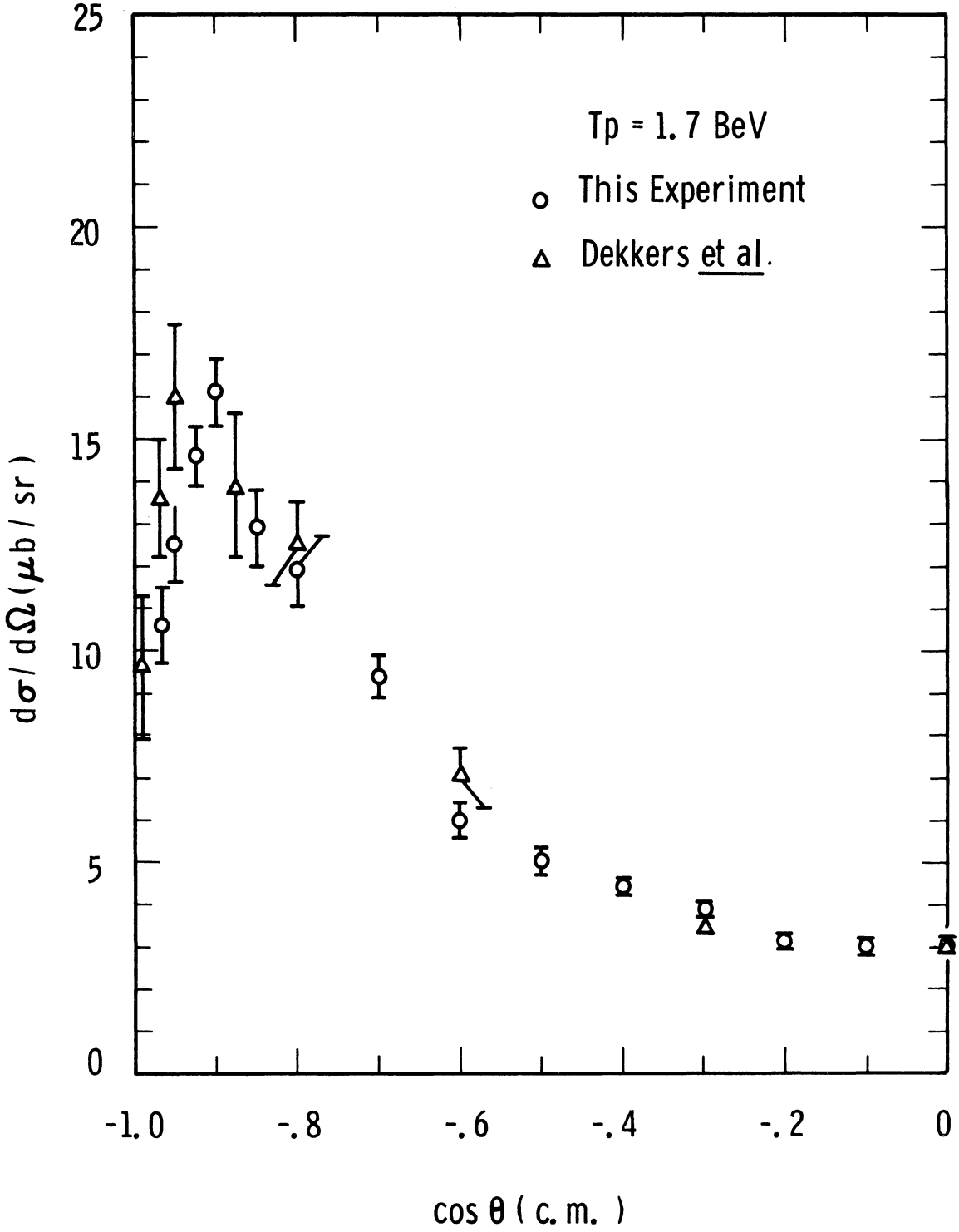

Fig. 18. Center of mass differential cross sections for the reaction $p+p \rightarrow d+\pi^+$ versus the cosine of the barycentric scattering angle at an incident proton kinetic energy of 1.7 BeV. The data shown are obtained from this experiment and deduced from the $\pi^+ + d \rightarrow p+p$ experiment of Dekkers et al.[15]

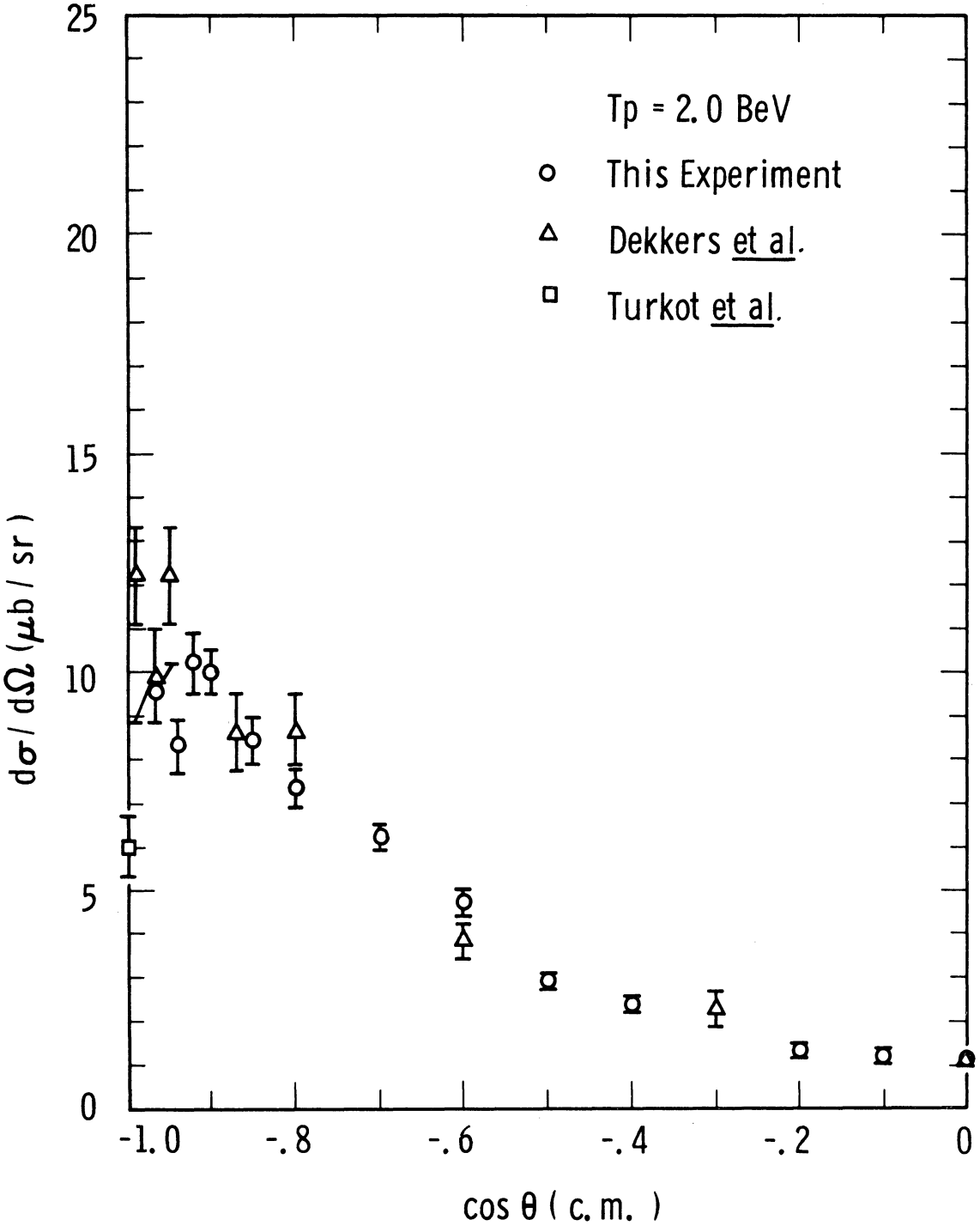

Fig. 19. Center of mass differential cross sections for the reaction $p+p \rightarrow d+\pi^+$ versus the cosine of the barycentric scattering angle at an incident proton kinetic energy of 2.0 BeV. The data shown are obtained from this experiment and from Turkot et al.[6] and deduced from the $\pi^+ + d \rightarrow p+p$ experiment of Dekkers et al.[15]

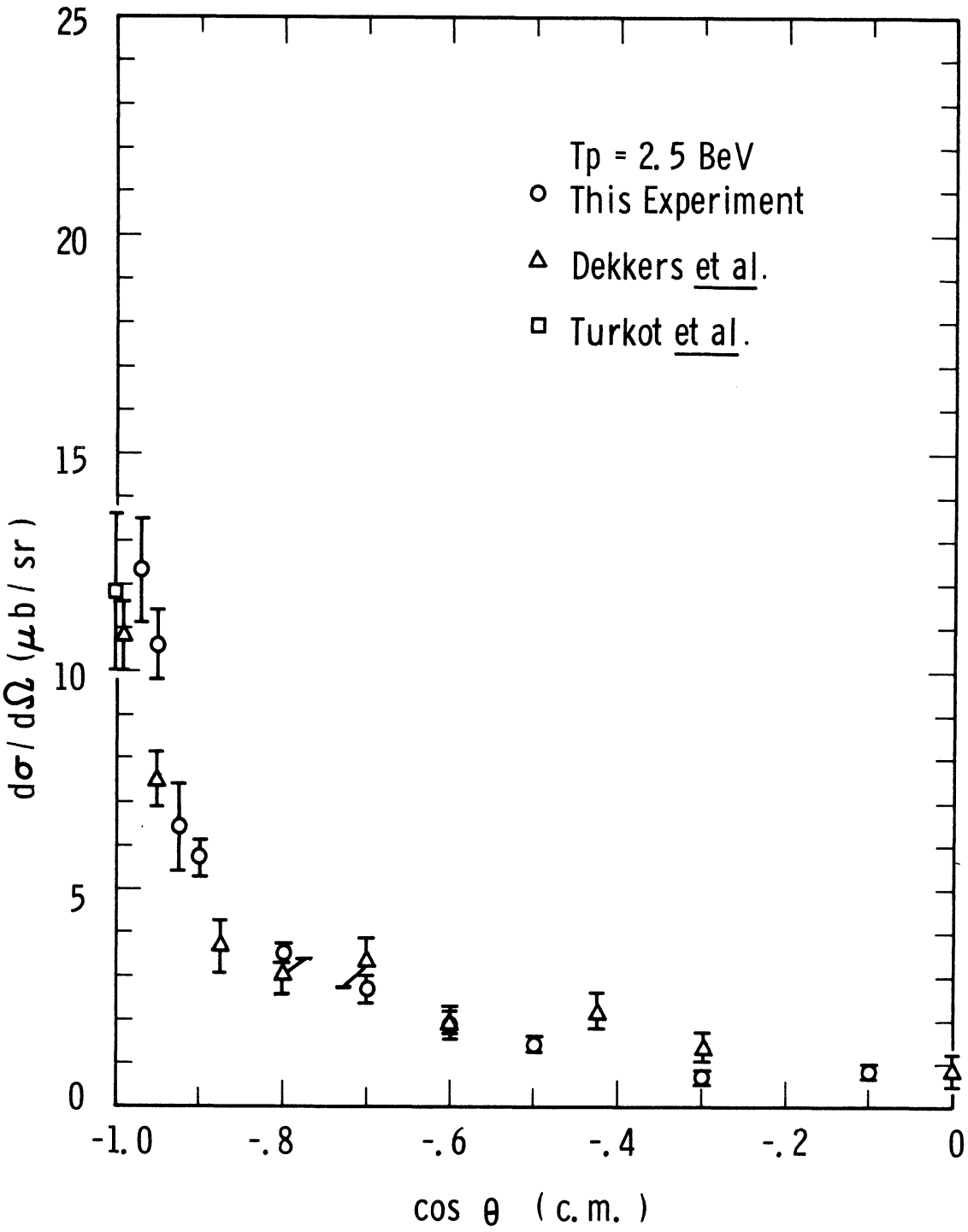

Fig. 20. Center of mass differential cross sections for the reaction $p+p \rightarrow d+\pi^+$ versus the cosine of the barycentric scattering angle at an incident proton kinetic energy of 2.5 BeV. The data shown are obtained from this experiment and from Turkot et al.[6] and deduced from the $\pi^+ + d \rightarrow p+p$ experiment of Dekkers et al.[15]

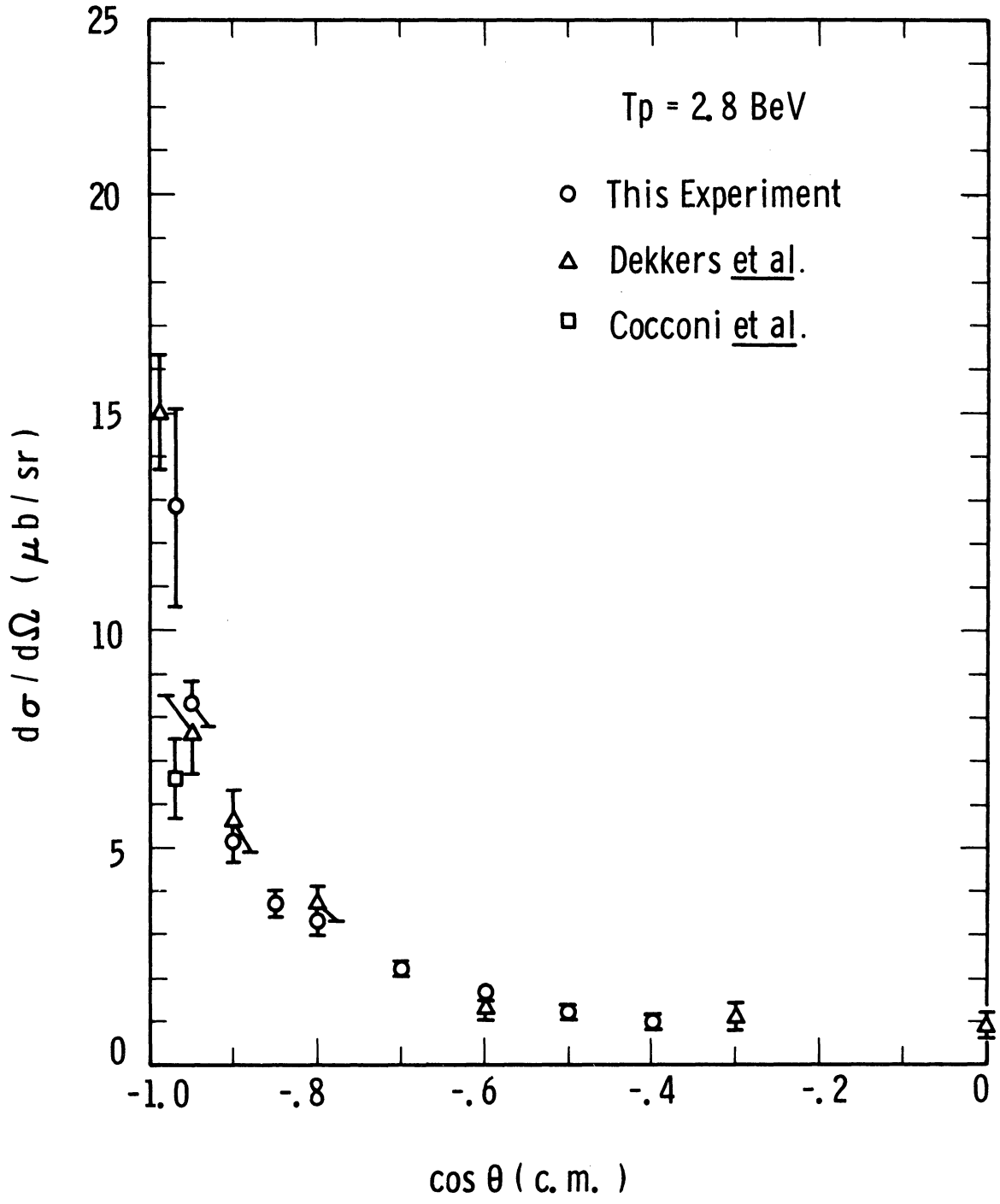

Fig. 21. Center of mass differential cross sections for the reaction $p+p \rightarrow d+\pi^+$ versus the cosine of the barycentric scattering angle at an incident proton kinetic energy of 2.8 BeV. The data shown are obtained from this experiment and Cocconi et al.[7] and deduced from the $\pi^+ + d \rightarrow p+p$ experiment of Dekkers et al.[15]

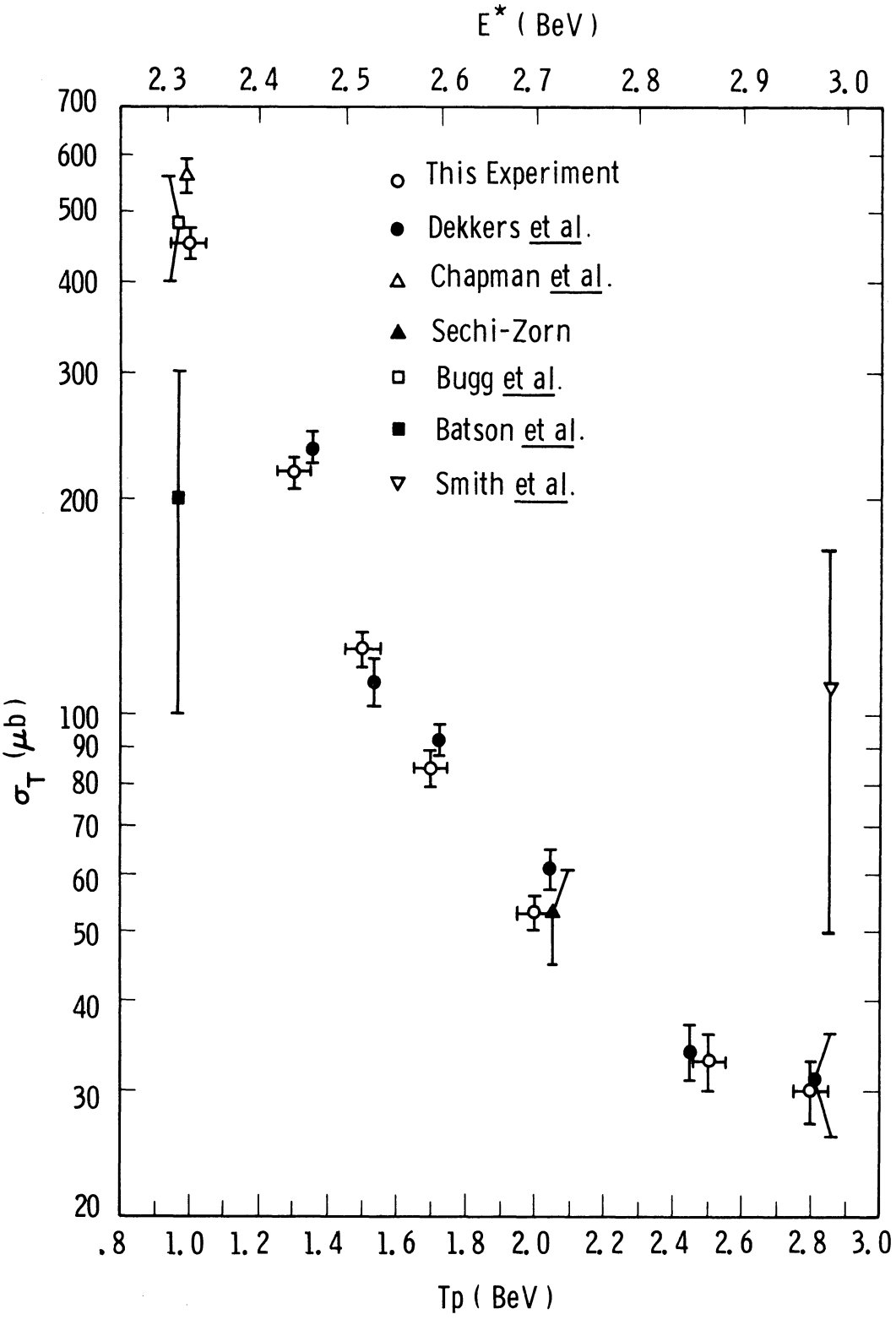

Fig. 22. Total cross sections for the reaction $p+p \rightarrow d+\pi^+$ versus the incident proton kinetic energy (lower abscissa) and the total barycentric energy (upper abscissa). The results of the experiment are shown by circles and are compared with the data of Dekkers et al.[15], Chapman et al.[12], Sechi-Zorn[13], Bugg et al.[10], Batson et al.[11], and Smith et al.[14]

VII. DISCUSSION AND CONCLUSION

From Figs. 15-21, it is seen that the recent data of Chapman *et al.*[12] and Dekkers *et al.*[15] agree reasonably well with the results of this experiment. At 1.0 BeV (Fig. 15), the differential cross sections from Chapman *et al.* are generally higher than ours, but this can be attributed to a slight difference in beam energies in the two experiments, since the cross sections decrease rapidly with an increase in the beam energy and there is an uncertainty of the beam energy in this experiment. Neither Chapman *et al.* nor we find a dip in the forward direction, as reported by Homer *et al.*[9] at .991 BeV. However, Homer *et al.* find this dip by measuring the deuteron momentum spectrum at a fixed laboratory angle (8.2°); the peak at the high-momentum end of this spectrum, corresponding to the $\pi^{+}d$ final state, is only .11 BeV away from the large proton momentum spectrum peak (at 8.2°) from elastic scattering. Proton contamination in the deuteron spectrum would explain the observed dip.

The results from Dekkers *et al.* confirm the striking feature of the angular distribution from 1.3 to 2.8 BeV which we find; as $\cos\theta$ varies from -0.5 to -1.0, the differential cross section rises, passes through a pronounced maximum, and then decreases rapidly. Moreover, this maximum in $d\sigma/d\Omega$ appears to migrate from $\cos\theta = -0.8$ at 1.3 BeV to $\cos\theta = -1.0$ at 2.5 BeV; i.e., at energies above 2.0 BeV the

turnover evolves into a peak at $\cos\theta = -1.0$. The $\cos\theta = -1.0$ measurements of Turkot et al.[6] at 1.5,2.1, and 2.5 BeV help to firmly establish this behavior.

The total cross section measurements (Fig. 22) show that the total cross section decreases rapidly and monotonically with energy from about 450 μb at 1.0 BeV to about 30 μb at 2.8 BeV. Except for the results from Batson et al.[11] and Smith et al.[14], both of which were based on less than ten events, the agreement among the various experiments is very good.

The data also show that the maximum in the forward differential cross section seen from combining the data of Turkot et al.[6] and Cocconi et al.[7] is caused by the energy dependence of the angular distribution and is not a manifestation of resonance behavior.

The energy dependence of $d\sigma/d\Omega$ near 90°, coupled with the smoothly varying angular distribution near 90°, is suggestive of a statistical interpretation.[4] However, the 90° cross section obtained in this experiment falls as $\exp(-8.15E)$, where E is the total c.m. energy, as opposed to the statistical model prediction of $\exp(-3.29E)$ (see p.24). Perhaps the energies of this experiment were too low for the statistical model to be applicable.

In Figs. 6-9, the one-pion exchange model theoretical curves (labeled P), as given by Yao[2], are compared with the data from this experiment. As pointed out by Yao and dis-

cussed in Chapter II, it is necessary to make several approximations to carry out the calculation; however, Yao has also failed to consider the effects of absorption in the initial and final states, making the calculation somewhat dubious. These uncertainties make a critical analysis of the model quite difficult. It is not inconsistent with the turnover, mentioned above, however.

The one-nucleon exchange model, developed in Chapter II, is successful in qualitatively explaining the two main features of the data. Figs. 3 and 4 illustrate the mechanism which creates the turnover and governs its propagation to $\cos\theta = -1.0$ as the beam energy is increased; this mechanism is based on the strong repulsive core which exists in the nucleon-nucleon central interaction potential. The other main feature of the data, the rapid decrease of the total cross section with energy, is explained by the decreasing probability for the occurrence of high momentum components in the momentum space deuteron wave function. The comparison of the model with the experimental data (Figs. 6-9, curves N) is not too favorable quantitatively; however, a more accurate deuteron wave function and a better treatment of the absorption phenomenon could make the agreement better. For example, at 2.8 BeV (Fig. 9) the turnover is still present in the theoretical curve; using a slightly larger hard core in the interaction potential could correct this, though, since increasing the core radius shifts the minimum in $F(\kappa)$ (see Fig.

3) to the left. (Using the Yukawa theory, Gartenhaus[34] has calculated the nucleon-nucleon potential through the fourth order in the coupling constant and finds a repulsive core of radius r_c = .71 F, as opposed to r_c = .65 F used in Fig. 9.)

A complete theoretical treatment of the reaction $p+p \rightarrow d+\pi^+$ should consider other production mechanisms, such as isotopic spin 1/2 isobar exchange, as well as removing uncertainties which exist in the one-pion exchange and one-nucleon exchange calculations. However, the qualitative success of the one-nucleon exchange model indicates that the one-nucleon exchange process could conceivably be the dominant mechanism in the reaction $p+p \rightarrow d+\pi^+$ from 1 to 2.8 BeV, and with suitable refinements of the calculation presented in this paper, the model could agree quantitatively with the data of this experiment.

APPENDIX

In the Appendix, we will evaluate the square of the matrix element M, doing the sum over initial proton and final deuteron spins. We have $M=M_1-M_2$

where

$$M_1=\sqrt{2}\ G\left[\frac{1}{i\not{n}_1+M+i\epsilon}\ \gamma_5 u(p_2)\right]^T\bar{\Gamma}u(p_1)$$

and M_2 is M_1 with $p_1\longleftrightarrow p_2$ and $n_1\longleftrightarrow n_2$.

Let

$$J=\frac{1}{4}\Sigma M_1^{\dagger} M_1$$

and

$$K=\frac{1}{4}\Sigma M_2^{\dagger} M_1.$$

Then

$$J=\frac{G^2}{2(n_1^2+M^2)^2}\ \Sigma\bar{u}(p_1)\Gamma(n_1)\gamma_4\Big[(-i\not{n}_1+M)\gamma_5 u(p_2)\bar{u}(p_2)$$
$$\gamma_4\gamma_5(-i\not{n}_1+M)^{\dagger}\Big]^T\bar{\Gamma}(n_1)u(p_1)$$

and

$$K=\frac{G^2}{2(n_1^2+M^2)(n_2^2+M^2)}\ \Sigma\bar{u}(p_2)\Gamma(n_2)\gamma_4\Big[(-i\not{n}_1+M)\gamma_5 u(p_2)\bar{u}(p_1)$$
$$\gamma_4\gamma_5(-i\not{n}_2+M)^{\dagger}\Big]^T\bar{\Gamma}(n_1)u(p_1).$$

Using the expressions for Γ from Chapter II and doing the proton spin sums, we obtain

$$J=-A_o\sum_{\substack{\text{deut}\\ \text{spin}}}\ \mathrm{Tr}\Big[(M_d-i\not{a})(\gamma\cdot\epsilon)(+i\not{n}_1+M)(-i\not{p}_2+M)$$
$$(i\not{n}_1+M)(\gamma\cdot\epsilon^*)(M_d-i\not{a})(-i\not{p}_1+M)\Big],$$

and

$$K=-C_o\sum_{\substack{\text{deut}\\\text{spin}}} \mathrm{Tr}\Big[(\gamma\cdot\epsilon)(M_d-i\not{d})(-i\not{p}_1+M)(i\not{n}_2+M)$$
$$(\gamma\cdot\epsilon^*)(M_d-i\not{d})(-i\not{p}_2+M)(i\not{n}_1+M)\Big],$$

where

$$A_o=\frac{\alpha G^2\pi F^2(n_1)}{8M^4M_d{}^2(1-\alpha\rho)(n_1{}^2+M^2)^2}$$

and

$$C_o=\frac{\alpha G^2\pi F(n_1)F(n_2)}{8M^4M_d{}^2(1-\alpha\rho)(n_1{}^2+M^2)(n_2{}^2+M^2)}\ .$$

Using $\not{a}\not{b}=-\not{b}\not{a}+2a\cdot b$

and $\sum_{\substack{\text{deut}\\\text{spin}}}(A\cdot\epsilon)(B\cdot\epsilon^*)=A\cdot B+\frac{(A\cdot d)(B\cdot d)}{M_d{}^2}$

where d is the four-momentum of the deuteron and A, B, a, and b are arbitrary four-vectors, we find

$$J=24(MM_d-p_1\cdot d)(\mu^2p_2\cdot d+2k\cdot p_2k\cdot d-M\mu^2M_d)A_o$$

and
$$K=8\Big[M^2M_d{}^2\mu^2-MM_d\mu^2(p_2\cdot d+p_1\cdot d)-(k\cdot d)^2(M^2+p_1\cdot p_2)$$
$$-MM_dk\cdot d(p_1\cdot k+p_2\cdot k)+\mu^2(p_1\cdot d)(p_2\cdot d)$$
$$+(p_1\cdot k)(p_2\cdot d)(k\cdot d)+(p_1\cdot d)(p_2\cdot k)(k\cdot d)\Big]C_o.$$

Since $|M|^2=M_1^\dagger M_1+M_2^\dagger M_2-M_1^\dagger M_2-M_2^\dagger M_1$, the terms $M_2^\dagger M_2$ and $-M_1^\dagger M_2$ can be obtained by making trivial changes in J and K, and the final expression obtained for $\frac{1}{4}\Sigma|M|^2$ is that given in Chapter II.

BIBLIOGRAPHY

1. M. L. Perl, L. W. Jones and C. C. Ting, Phys. Rev. 132, 1273 (1963).

2. T. Yao, Phys. Rev. 134, B454 (1964).

3. J. Chahoud, G. Russo, and F. Selleri, Phys. Rev. Letters 11, 506 (1963).

4. G. Fast and R. Hagedorn, Nuovo Cimento 27, 208 (1963).

   G. Fast, R. Hagedorn, and L. W. Jones, Nuovo Cimento 27, 856 (1963).

   L. W. Jones, Phys. Letters 8, 287 (1964).

5. R. Hagedorn, CERN preprint 9019/TH.433 (1964).

6. F. Turkot, G. B. Collins and T. Fujii, Phys. Rev. Letters 11, 474 (1963).

7. G. Cocconi, E. Lillethun, J. P. Scanlon, C. A. Stahlbrandt. C. C. Ting, J. Walters and A. M. Wetherell, Phys. Letters 7, 222 (1963).

8. M. G. Mescheryakov, B. S. Neganov, N. P. Bogachev, V. M. Sidorov, Dokl. Akad. Nauk-SSSR, 100, 673 (1955).

9. R. J. Homer, Q. H. Khan, W. K. McFarlane, J. S. C. McKee, A. W. O'Dell, L. Riddiford and P. G. Williams, Phys. Letters 9, 72 (1964).

10. D. V. Bugg, A. J. Oxley, J. A. Zoll, J. G. Rushbrook, V. E. Barnes, J. B. Kinson, W. P. Dodd, G. A. Doran, and L. Riddiford, Phys. Rev. 133, B1017 (1964).

11. A. P. Batson, B. B. Culwick, J. G. Hill, and L. Riddiford, Proc. Roy. Soc. (London) A251, 218 (1959).

12. K. R. Chapman, T. W. Jones, Q. H. Khan, J. S. McKee, H. B. Van Der Raay, and T. Tanimura, Phys. Letters 11, 253 (1964).

13. B. Sechi-Zorn, Bull. Am. Phys. Soc. 7, 349 (1962).

14. G. A. Smith, H. Courant, E. C. Fowler, H. Kraybill, J. Sandweiss, and H. Taft, Phys. Rev. 123, 2160 (1961).

15. D. Dekkers, B. Jordan, R. Mermod, C. C. Ting, G. Weber, T. R. Willitts, and K. Winter, Phys. Letters 11, 161 (1964).

16. W. O. Lock, High Energy Nuclear Physics (John Wiley and Sons Inc., New York, 1960), p.28.

17. J. Bernstein, Phys. Rev. 129, 2323 (1963).

18. J. Nearing, Phys. Rev. 132,2323 (1963).

19. V. Cook, B. Cork, W. R. Holley, and M. Perl, Phys. Rev. 130, 762 (1963).

20. see, for example, W. Tobocman, Theory of Direct Nuclear Reactions (Oxford University Press, New York, 1961).

21. R. Blankenbecler, M. L. Goldberger, and F. R. Halpern, Nucl. Phys. 12, 629 (1959).

22. M. L. Goldberger, Y. Nambu, and R. Oehme, Ann. Phys. 2, 226 (1957).

23. G. F. Chew and M. L. Goldberger, Phys. Rev. 77, 470 (1950).

24. L. Hulthén and M. Sugawara, Handbuch der Physik XXXIX, 1, Springer-Verlag, Berlin, Göttingen, Heidelberg 1957.

25. R. Blankenbecler and L. F. Cook, Jr., Phys. Rev. 119, 1745 (1960).

26. E. E. Salpeter and J. S. Goldstein, Phys. Rev. 90, 983 (1953).

27. Marc H. Ross and Gordon L. Shaw, Phys. Rev. Letters 12, 627 (1964).

28. Loyal Durand and Yam Tsi Chiu, Phys. Rev. Letters 12, 399 (1964).

29. A. Dar and W. Tobocman, Phys. Rev. Letters 12, 511 (1964).

30. K. Gottfried and J. D. Jackson, Phys. Letters 8, 144 (1964).

31. T. Fujii, G. B. Chadwick, G. B. Collins, P. J. Duke, N. C. Hien, M. A. R. Kemp, and F. Turkot, Phys. Rev. 128, 1836 (1962).

32. R. Jastrow, Phys. Rev. 81, 165 (1951).

33. J. L. Gammel, R. S. Christian, and R. M. Thaler, Phys. Rev. 105, 311 (1957).

34. S. Gartenhaus, Phys. Rev. 100, 900 (1955).

K. Brueckner and K. Watson, Phys. Rev. 92, 1023 (1953).

M. M. Levy, Phys. Rev. 84, 441 (1951).

35. G. B. Chadwick, G. B. Collins, P. J. Duke, T. Fujii, N. C. Hien, M. A. R. Kemp, and F. Turkot, Phys. Rev. 128, 1823 (1962).

36. J. A. Helland, T. J. Devlin, D. E. Hagge, M. J. Longo, B. J. Moyer, and C. D. Wood, Phys. Rev. 134, B1062 (1964).

37. J. A. Helland, C. D. Wood, T. J. Devlin, D. E. Hagge, M. J. Longo, B. J. Moyer, and V. Perez-Mendez, Phys. Rev. 134, B1079 (1964).

38. B. J. Moyer, private communication. I would like to thank Dr. Moyer for sending me cross sections for the reaction $\pi^- + p \rightarrow \pi^0 + n$ prior to publication.

39. L. Bertanza, R. Carrara, A. Drago, P. Franzini, I. Mannelli, G. Silvestrini, and P. H. Stoker, Nuovo Cimento 19, 467 (1961).

40. J. J. Livingood, Principles of Cyclic Particle Accelerators (D. Van Nostrand Co., Inc., 1961), p.314.

41. G. W. Bennett, Cosmotron Internal Report #GWB-2.

42. D. M. Ritson, Techniques of High Energy Physics (Interscience publishers, 1961), p.449.

43. R. Sugarman, F. C. Merritt, and W. A. Higginbotham, Nanosecond Counter Circuit Manual, Brookhaven National Laboratory Report BNL711(T-248), unpublished (1962).

44. A. M. Poskanzer, L. P. Remsberg, S. Katcoff, and J. B. Cumming, Phys. Rev. 133, B1507 (1964).

45. J. B. Cumming, G. Friedlander, and C. E. Swartz, Phys. Rev. 111, 1386 (1958).

46. J. B. Cumming, A. M. Poskanzer, and J. Hudis, Phys. Rev. Letters 6, 484 (1961).

47. J. B. Cumming, J. Hudis, A. M. Poskanzer, and S. Kaufman, Phys. Rev. 128, 2392 (1962).

48. B. Rossi, High Energy Particles (Prentice-Hall Inc., New York, 1952), p. 448.

49. F. F. Chen, C. P. Leavitt, and A. M. Shapiro, Phys. Rev. 103, 211 (1956).

50. V. S. Barashenkov, Ob'edinennyi Institut Yadernykh Issledovaniy preprint, 1960.

51. J. Askin, T. Fazzini, G. Fidecaro, Y. Goldschmidt-Clermont, N. H. Lipman, A. W. Merrison, and H. Paul, Nuovo Cimento 16, 490 (1960).

52. O. E. Overseth, R. M. Heinz, L. W. Jones, M. J. Longo, D. E. Pellett, M. L. Perl, and F. Martin, Phys. Rev. Letters 13, 59 (1964).